The mitochondrial stress-induced protein carboxyl-terminal alanine and threonine tailing (msiCAT-tailing) promotes glioblastoma tumorigenesis by modulating mitochondrial functions

Ting Cai[1,†], Bei Zhang[1,†], Esha Reddy[1], Yuanna Wu[1], Yinglu Tang[1], Isha Mondal[2], Jerry Wang[1,‡], Winson S Ho[2], Rongze Olivia Lu[2,*], Zhihao Wu[1,*]

[1] Department of Biological Sciences, Dedman College of Humanities and Sciences, Southern Methodist University, Dallas, TX 75275, USA.

[2] Department of Neurological Surgery, University of California, San Francisco, CA 94143, USA

[†] These authors contributed equally.

[‡] Current address: McCombs School of Business, University of Texas at Austin, Austin, TX 78712, USA

* Correspondence authors: Rongze Olivia Lu (rongze.lu@ucsf.edu); Zhihao Wu (zhihaowu@smu.edu)

16 **Highlights**

17 - The RQC pathway is disturbed in glioblastoma (GBM) cells
18 - msiCAT-tailing on ATP5α elevates mitochondrial membrane potential and inhibits MPTP
19 opening
20 - msiCAT-tailing on ATP5α inhibits drug-induced apoptosis in GBM cells
21 - Inhibition of msiCAT-tailing impedes overall growth of GBM cells

22

Abstract

The rapid and sustained proliferation in cancer cells requires accelerated protein synthesis. Accelerated protein synthesis and disordered cell metabolism in cancer cells greatly increase the risk of translation errors. ribosome-associated quality control (RQC) is a recently discovered mechanism for resolving ribosome collisions caused by frequent translation stalls. The role of the RQC pathway in cancer initiation and progression remains controversial and confusing. In this study, we investigated the pathogenic role of mitochondrial stress-induced protein carboxyl-terminal terminal alanine and threonine tailing (msiCAT-tailing) in glioblastoma (GBM), which is a specific RQC response to translational arrest on the outer mitochondrial membrane. We found that msiCAT-tailed mitochondrial proteins frequently exist in glioblastoma stem cells (GSCs). Ectopically expressed msiCAT-tailed mitochondrial ATP synthase F1 subunit alpha (ATP5α) protein increases the mitochondrial membrane potential and blocks mitochondrial permeability transition pore (MPTP) formation/opening. These changes in mitochondrial properties confer resistance to staurosporine (STS)-induced apoptosis in GBM cells. Therefore, msiCAT-tailing can promote cell survival and migration, while genetic and pharmacological inhibition of msiCAT-tailing can prevent the overgrowth of GBM cells.

Key words

Glioblastoma (GBM); ribosome-associated quality control (RQC); mitochondrial stress-induced protein carboxyl-terminal terminal alanine and threonine tailing (msiCAT-tailing); ATP synthase F1 subunit alpha (ATP5α); mitochondrial membrane potential; mitochondrial permeability transition pore (MPTP); apoptosis

Introduction

Proteins are the molecular basis of life activities. Excessive protein synthesis is particularly important in rapidly dividing cells, such as cancer cells. To cope with this demand, cancer cells extensively regulate the initiation, elongation and termination of their protein translation (1). However, increased protein translation also proportionally accumulates the likelihood of translation errors (2). Combined with the significant changes in cellular metabolism, such as energy fluctuations and redox state shifts, how to respond to various sudden abnormal events during the protein translation process becomes essential. Ribosome-associated quality control (RQC) is a recently discovered class of mechanisms in eukaryotic cells that sense and rescue ribosome decelerations, stalls, and even collisions that occur during translation elongation or termination steps (3, 4).

RQC consists of a sequence of molecular events. The first is that the ZNF598/RACK1 complex recognizes the characteristic 40S-40S interface formed by collided ribosomes and promotes the ubiquitination of specific 40S subunit proteins (5, 6). Subsequently, the ASC-1 complex dissociates the leading collided ribosome (7, 8). Events that occur thereafter include: ribosomal subunit splitting and recycling (9), modification of the nascent peptide chains through the C-terminal alanine and threonine (CAT-tailing) mechanism (10), release of CAT-tailed products from the 60S subunits by ANKZF1/VMS1 (11), and degradation of aberrant peptides by the Ltn1/VCP/NEMF complex (4). The biological significance of the CAT-tailed translation products generated in the RQC remains unclear. On one side of the coin, CAT-tails can push lysine residues out of the ribosome exit channel to achieve Ltn1-mediated ubiquitination (12), or promote degradation of faulty nascent peptide chains (13, 14); on the other side, CAT-tailed proteins are prone to form detergent-insoluble aggregates (15, 16). In addition, depending on the

71 nature and subcellular localization of the original target, CAT-tailed proteins may also have
72 unique functions, but this is currently poorly understood. Importantly, CAT-tailed proteins have
73 been found in a variety of human neurodegenerative diseases and are believed to play important
74 roles in their pathogenesis (17-19).

75 The increased abnormalities in translation have been found in cancer cells, such as stop
76 codon readthrough (20), frame-shifting (21), and oxidative stress-induced ribosome stalling (22),
77 indicating the possible involvement of the RQC pathway. However, despite the detection of
78 CAT-tail modification on mitochondrial proteins caused by impaired RQC in HeLa cells (17),
79 there is still a lack of mechanistic studies on the role of RQC factors in cancer biology. The
80 expression of many RQC factors (*e.g.*, ASCC3, ABCE1, ANKZF1 and VCP) has been shown to
81 be dysregulated in cancer cells (23-26). Intriguingly, different RQC factors, or even the same
82 factor, may exhibit completely opposite functions in oncogenesis and tumor suppression under
83 distinct conditions. Inhibition of ABCE1, ASCC3 and VCP inhibits cancer cell growth and
84 survival (23, 24, 26), whereas inhibition of NEMF/Clbn and ZNF598 may promote cancer
85 growth and survival (27, 28). This suggests that the role of RQC factors in cancer cells is
86 sophisticated and highly genetic and environmental context dependent. A recent study
87 investigated the mechanism of ANKZF1 in mitochondrial proteostasis and its impact on the
88 malignant progression of GBM (29). However, the nonphysiologically mitochondria-targeted
89 GFP was used in the study to induce the matrix proteotoxicity, and the role of endogenous
90 mitochondrial proteins in this process remains unclear.

91 The co-translational import defects triggered by mitochondrial stress induce CAT-tailing
92 not only on the mitochondrial C-I30 protein (complex-I 30 kD subunit protein, also known as
93 NDUFS3), but also widely on other nuclear genome-encoded mitochondrial proteins (17, 30).

94 How these mitochondrial stress-induced CAT-tailed (msiCAT-tail) proteins participate in and
95 influence the core of mitochondrial biology has not yet been studied. Since CAT-tailing imparts
96 new properties to target proteins, it is likely to contribute to some unique characteristics of
97 cancer cell mitochondria, such as mitochondrial hyperpolarization (31, 32) and high
98 mitochondrial membrane potential-related resistance to drug-induced apoptosis (33-35).
99 Mitochondrial membrane potential is formed by the proton (H^+) concentration gradient across
100 the mitochondrial inner membrane. It is generated and maintained by oxidative phosphorylation
101 (OXPHOS), in which H^+ ions are shuttled through the electron transport chain composed of four
102 complexes (I to IV), resulting in the accumulation of H^+ in the intermembrane space (36). ATP
103 synthase (complex-V) then harnesses the energy from the H^+ gradient by promoting its influx
104 into the mitochondrial matrix and produces ATPs in the process (37). Despite increased
105 metabolic demands, many cancer cells have reduced OXPHOS (38). It remains unclear how
106 cancer cells maintain or even increase mitochondrial membrane potential in the absence of
107 OXPHOS (31).

108 In this study, we focused on msiCAT-tailing modification on the mitochondrial ATP
109 synthase F1 subunit alpha (ATP5α). We observed that msiCAT-tailed ATP5α is present in GBM.
110 The short-tailed ATP5α can incorporate into the ATP synthase, increase mitochondrial membrane
111 potential, and inhibit the assembly and opening of mitochondrial permeability transition pore
112 (MPTP). Therefore, the presence of msiCAT-tailed ATP5α enhances the resistance of GBM cells
113 to staurosporine (STS)- and temozolomide (TMZ)-induced programmed cell death and promotes
114 cancer cell survival, proliferation, and migration. Conversely, inhibition of msiCAT-tailing
115 suppresses cancer cell growth and resensitizes GBM cells to apoptosis. Our study elucidates the
116 role of CAT-tailed mitochondrial proteins in cancer cells, reveals the importance of the RQC

117 pathway in cancer biology, and indicates that components and products in the RQC pathway may

118 be effective therapeutic targets for GBM.

Results

Presence of mitochondrial stress-induced protein carboxyl-terminal terminal alanine and threonine tailing (msiCAT-tailing) in glioblastoma cells

Dysregulation of individual factors associated with ribosome-associated quality control (RQC) has been described in a variety of cancer cells such as prostate cancer, adenocarcinoma, non-small cell lung cancer and colon cancer cells (23-26), but an overall characterization of the RQC pathway genes has not been performed. We first performed differential expression analysis using the transcriptomic data between 153 glioblastoma (GBM) patients and 206 healthy controls from public datasets (39). We found that compared with normal subjects, the expression levels of genes related with the RQC pathway such as *ABCE1*, *ASCC1*, *ASCC2*, *ASCC3*, *RACK1*, and *VCP* were significantly elevated (logFC > 1; adj.P.Val < 0.001) in GBM cells, whereas *ANKZF1* was the only gene whose expression level (logFC = -0.43, adj.P.Val = 0.0005) was downregulated (Fig. 1A, Table S1). Changes in these genes imply activation of the RQC pathway and accumulation of CAT-tailed protein. The msiCAT-tailed mitochondrial protein C-I 30 (complex-I 30 kD subunit, also known as NDUFS3) was previously discovered in HeLa (cervical cancer) cells as the endogenous substrate of RQC (17). We wanted to know whether C-I 30 and other msiCAT-tailed proteins are indeed present in GBM cells. Patient-derived GBM stem cells (pGSCs), but not normal neural stem cells (NSCs), displayed several msiCAT-tailed mitochondrial proteins, such as C-I30, COX4 (cytochrome c oxidase subunit 4), and ATP5α (ATP synthase F1 subunit alpha). In line with the detectable msiCAT-tailed proteins in pGSCs, we also found elevated levels of NEMF (nuclear export mediator factor) (10) but decreased expression of ANKZF1 (ankyrin repeat and zinc-finger peptidyl tRNA hydrolase 1) (11), indicating an increase in CAT-tailing activation, which is similar to the results of bioinformatics

142 analysis in GBMs (Fig. 1B). In the following experiments, we selected two GBM cell lines,
143 SF268 (labeled as SF cells in figures) (40) and GSC827 (41) with more stem cell characteristics,
144 and two control cell lines SVG p12 (abbreviated as SVG) and Normal Human Astrocytes
145 E6/E7/hTERT (abbreviated as NHA) (42). We also examined their expression of RQC proteins
146 (Fig. S1A). Similar to the results with patient-derived GSC cells, we also observed decreased
147 ANKZF1 expression and increased ASCC3 in GSC827 and SF268 cells. Although there was no
148 obvious change in NEMF expression, we found modification on NEMF (indicated by *) in
149 GSC827 cells, hinting its possible functional changes (Fig. S1A). In line with this, we used non-
150 stop protein translation system to induce CAT-tailing on Flag tagged β-globin reporter in GBM
151 and control cells (43). We are surprised to observe that the translation rate of GBM cells for
152 normal proteins (β-globin-control) actually decreased compared to control cells, the RQC system
153 in GBM cells could produce significantly more CAT-tailed protein (β-globin-nonstop); and this
154 process can be inhibited by the CAT-tailing elongation inhibitor anisomycin (44) (Fig. 1C).

155 We next wanted to know the biological consequences of generating these CAT-tailed
156 mitochondrial proteins. The heterogeneity of CAT-tailing toward substrates and tail lengths
157 makes it difficult to study the function of specific CAT-tail-modified proteins. In our previous
158 study, adding the AT repeat tails to the C-terminus of mitochondrial proteins can effectively
159 simulate a CAT-tail like reaction (17). Among the CAT-tailed mitochondrial targets we found,
160 ATP5α is one of those with the highest abundance in functional mitochondria (45) and has
161 additional critical roles in cancers (46). We therefore wondered what unique functions CAT-
162 tailed ATP5α might provide. To test it, in control (SVG and NHA) and GBM (SF268 and
163 GSC827) cell lines, we overexpressed ATP5α proteins having artificial CAT-tails: ATP5α-AT3
164 containing three alanine-threonine repeats and ATP5α-AT20 that contains containing twenty

165 alanine-threonine repeats. Consistent with previous observations, long CAT-tailed but not short
166 CAT-tailed proteins, has post-translational modifications and detergent-insoluble aggregates that
167 appear as slower migrating bands and high molecular weight smeared signals in protein
168 electrophoresis (Fig. 1D). Notably, compared with the control cells (SVG, NHA), the GBM cell
169 lines (GSC827, SF268) expressed more ATP5α-AT20 proteins, indicating that GBM cells have
170 more capability to deal with protein aggregation (Fig. 1D, ratios). In addition, cytological
171 analysis tells us that the short AT tail does not significantly affect subcellular localization. Like
172 the tailless ATP5α protein, ATP5α-AT3 is mainly located in mitochondria, while a significant
173 proportion of ATP5α-AT20 appears in the cytoplasm near mitochondria and forms protein
174 aggregates (Fig. S1B). Moreover, the proportion of cells having protein aggregates was highest
175 in GSC cells, which are the most malignant (Fig. S1C). Importantly, not only exogenously
176 expressed tailed proteins, endogenous ATP5α also formed protein aggregates attached to
177 mitochondria (outer membrane) in some GBM cells (Fig. 1E, 1F). Taken together, we found
178 evidence showing the existence of RQC dysregulation and msiCAT-tailing occurring in GBM
179 cells.

180

181 **msiCAT-tailed ATP5α elevates mitochondrial membrane potential (ΔΨm)**

182 Cancer cells can keep their mitochondrial membrane potential (ΔΨm) stable, sometimes even
183 elevated, while their respiration is reduced. We first confirmed this phenomenon in patient-
184 derived pGSC cells, which had a higher membrane potential but lower ATP production than
185 control NSC cells (Fig. 2A, 2B). We also tested our GBM cell lines (GSC827, SF268) and the
186 control cell line NHA (42). We found that both GSC and SF268 exhibited comparable or higher

187 membrane potential than NHA cells (Fig. S2A), while their mitochondrial ATP levels were lower
188 (Fig. S2B, S2C). Inhibiting msiCAT-tailing using genetic approaches, such as knocking down
189 NEMF (sgNEMF) and overexpressing ANZKF1 (oeANZKF1), effectively reduced the
190 mitochondrial membrane potential in GBM but not NHA cells (Fig. 2C, S2D).

191 We next wanted to determine how msiCAT-tailed proteins significantly impact
192 mitochondrial functions. We ectopically expressed ATP5α-AT3 and ATP5α-AT20 (Flag tagged)
193 proteins in GBM and control cell lines. We found that they both can increase mitochondrial
194 membrane potential in GBM but not NHA cells (Fig. 2D). Intriguingly, Blue Native
195 Polyacrylamide Gel Electrophoresis (BN-PAGE) analysis indicated that CAT tails of different
196 lengths exert distinct effects on mitochondria. ATP5α-AT3 proteins were incorporated into
197 mitochondrial respiratory chain complexes, while ATP5α-AT20 proteins formed high molecular
198 weight complexes or existed in monomers (Fig. 2E). As expected, long CAT-tails form protein
199 aggregates, which may cause proteostasis stress in mitochondria (17, 29). We next utilized the
200 Agilent Seahorse Cell Mitochondrial Stress Test to measure key parameters of mitochondrial
201 respiration by directly measuring the oxygen consumption rate (OCR) of cells. Interestingly, we
202 found that the expression of both ATP5α-AT3 and ATP5α-AT20 can impair mitochondrial
203 oxidative phosphorylation, resulting in decreased ATP synthesis, basal respiration, and maximum
204 respiration rates (Fig. 2F-2I). Collectively, these data indicated that expression of CAT-tailed
205 ATP5α protein significantly affects mitochondrial function. In comparison, short tails are more
206 likely to directly influence the function of ATP synthase, whereas long tails may cause
207 mitochondrial proteostasis stress thereby indirectly affecting mitochondrial respiration.

208

209 **msiCAT-tailed ATP5α regulates mitochondrial permeability transition pore (MPTP)**
210 **opening**

211 In addition to its primary function of generating ATP, recent studies have implicated F_1F_0 ATP
212 synthase may be an integral component of mitochondrial permeability transition pore (MPTP)
213 complex (47-49). If MPTP is affected by CAT-tailed components such as ATP5α, this may cause
214 dysregulation of its open-close state or assembly. Therefore, in the following experiments, we
215 investigated how msiCAT-tailing modulates the status of MPTP. By comparing the MPTP status
216 in GBM cells and control cells, we found that MPTP in GSC827 cells is largely in a close state.
217 Interestingly, the CAT-tailing inhibitor anisomycin can effectively eliminate the endogenous
218 ATP5α aggregation (Fig. S3A, S3B) and promote the opening of MPTP in GSC827 cells,
219 illustrated by the reduced Calcein signal (Fig. 3A, 3B). Short-term opening of MPTP promote the
220 efflux of proton, Ca^{2+} ions and other signaling molecules from the mitochondrial matrix (50).
221 Mitochondrial Ca^{2+} retention capacity (CRC) measurements have been used to calculate the
222 amount of Ca^{2+} ions needed to open MPTP, directly indicating their open-close states. We
223 observed that GSC827 cells establish higher CRC than NHA cells, and anisomycin pre-treatment
224 and NEMF knockdown significantly reduce the CRC, suggesting the opening of MPTP in GBM
225 cells upon elimination of CAT-tailed proteins (Fig. 3C, 3D).

226 To determine whether the CAT-tail modifications on ATP5α can modulate the open-close
227 state of MPTP, we compared the effects of artificial AT repeat tails on MPTP in GBM cells.
228 Interestingly, we found that the short AT tail (AT3) can inhibit the functional opening of MPTP,
229 while the long AT tail (AT20) has a weaker effect (Fig. 3E, 3F), which may be explained by their
230 differential involvement in ATP synthase (Fig. 2E). To gain a glimpse into the role of ATP5α
231 protein with different msiCAT-tails, we examined the interaction between ATP5α and two

232 known MPTP components Cyp-D and ANT2; however, no direct interaction was detected (Fig.
233 S3C). Interestingly, we found that Cyp-D expression is reduced in varying proportions, when
234 ATP5α-AT3 or ATP5α-AT20 is ectopically expressed, hinting reduced MPTP formation (Fig.
235 S3D). We then used BN-PAGE to detect the complex composed of ANT1/2. We found that the
236 presence of both ATP5α-AT3 and -AT20 significantly changed the pattern of ANT1/2-containing
237 complexes, with the expected bands disappearing (indicated by *) and aggregates forming at
238 high-molecular weight positions (Fig. 3G). It is worth mentioning that the ANT1/2 complex is in
239 close proximity to ATP synthase in the electrophoresis, supporting the hypothesis that ATP
240 synthase may be part of the MPTP supercomplex. In summary, we conclude that msiCAT-tailed
241 ATP5α proteins, especially the short-tailed (AT3) ones, incorporate into the ATP synthase and
242 regulate the MPTP status.

243

244 **msiCAT-tailing promotes GBM cells migration and enhances their resistance to apoptosis**

245 The high mitochondrial membrane potential and tightened MPTP conferred by msiCAT-tailed
246 ATP5α and other mitochondrial proteins may make cells more adaptable to stresses. Therefore,
247 we next wanted to know how the msiCAT-tailing mechanism affects GBM cells at the cellular
248 level. In the MTT assays (51), we observed that overexpression of the short AT repeat tail (AT3)
249 and the long AT repeat tail (AT20) fused with ATP5α significantly promotes GBM cell but not
250 NHA cell viability (Fig. 4A, 4B). Further, in *in vitro* transwell cell migration assays (52) and
251 wound healing experiments (53), we observed that that GBM cells overexpressing CAT-tailed
252 ATP5α showed stronger cell invasion ability and faster wound healing, indicating faster cell
253 migration occurs (Fig. 4C, 4D, S4A, S4B). It is worth mentioning that in ANKZF1 knockdown

254 U87 and U251 cell lines, the accumulation of abnormal mitoGFP can lead to a decrease in
255 cellular adaptability (29). We speculate that this is because the mitochondria of different cell
256 lines have different adaptability to proteostasis stress. One support was that in the initial
257 experiments, we did not find that the mild expression of ATP5α-AT3 and ATP5α-AT20 induces
258 strong mitochondrial proteotoxic responses, such as significantly up-regulated *LONP1*, *mtHSP70*
259 and *HSP60* mRNA level (Fig. S4C).

260 In addition to this, we found that GBM cells are more resistant to staurosporine (STS)-
261 induced apoptosis, as evidenced by reduced TUNEL-positive cells (Fig. S4D, S4E) and
262 significantly weakened cleavage of Poly (ADP-ribose) polymerase (PARP-1) proteins (Fig. S4F)
263 (54). To confirm whether CAT-tailed ATP5α proteins contribute to resistance to apoptosis, we
264 further overexpressed these proteins in GBM cells. We found that both short tail (ATP5α-AT3)
265 and long tail (ATP5α-AT20) can effectively enhance cells resistance to STS-induced apoptosis,
266 proving that protein CAT-tailation caused may be closely related to tumorigenesis (Fig. 4E, 4F).
267 Consistent with this, we found that overexpression of artificial CAT-tailed ATP5α proteins, also
268 enhance the resistance of GBM cells to temozolomide (TMZ)-induced apoptosis (Fig. 4G).
269 Combining these data, we demonstrate that RQC-induced CAT-tailing on ATP5α protein may
270 contribute to the resistance of GBM cells to drug-induced apoptosis.

271

272 **Inhibiting the RQC pathway impedes GBM cell progression**

273 Through previous studies, we confirmed the importance of the RQC pathway mediated msiCAT-
274 tailing mechanism mediated for GBM progression. Therefore, inhibiting the RQC pathway may
275 be a potentially effective means to combat GBM. To test this hypothesis, we first treated patient-

276 derived pGSC cells with the CAT-tailing inhibitor anisomycin. We found that the pGSC cell lines
277 were more sensitive to anisomycin treatment than control NSC cells (Fig. 5A). Similarly, by
278 knocking down NEMF (sgNEMF) or overexpressing ANKZF1 (oeANZKF1) in GBM cell line
279 (SF268), we found that genetically inhibiting the RQC pathway can also inhibit GBM growth
280 (Fig. 5B). Notably, the growth of NHA cells as a control was also inhibited, indicating that these
281 two genes are critical factors in general cell proliferation (Fig. S5A). The RQC pathway has a
282 more significant impact on the migration ability of GBM cells. In transwell *in vitro* cell
283 migration assays, sgNEMF or oeANZKF1 significantly inhibited the migration of GBM cells but
284 had no effect on NHA cells (Fig. 5C, 5D). Similarly, GSC cells but not NHA cells treated with
285 anisomycin also significantly weakened their cell migration ability (Fig. S5B, S5C).

286 Next, we studied the effect of RQC pathway on the anti-apoptosis of GBM cells. The first
287 thing we discovered were changes in mitochondrial function. Previously, genetic inhibition of the
288 RQC pathway (sgNEMF or oeANKZF1) could significantly reduce the membrane potential of
289 GBM mitochondria (Fig. 2C); anisomycin treatment also has the same effect here (Fig. 5E). We
290 also found that in GSC cells, anisomycin treatment could promote MPTP opening, but not in
291 NHA cells (Fig. 3A). Correspondingly, inhibition of the RQC pathway with anisomycin rendered
292 GBM cell lines more sensitive to STS-induced apoptosis, as evidenced by more PARP-1
293 cleavage and TUNEL-positive signals (Fig. 5F-5H). Similarly, genetic inhibition of the RQC
294 pathway could achieve the similar sensitization (Fig. S5D, S5E). Finally, we found that the RQC
295 pathway also plays a role in TMZ-induced cell death. For example, co-treatment of anisomycin
296 and TMZ significantly inhibited the survival of GBM cell lines (Fig. 5I) and effectively inhibited
297 the size of spheroids formed by GSC cells (Fig. 5J and 5K). In conclusion, the activity of the
298 RQC pathway is important for GBM progression, including their proliferation, migration, and

299 survival upon induction of apoptosis.

300

301 **Discussion**

302 In this study, we mainly explored the role of RQC and its products, especially the mitochondrial
303 proteins modified by the msiCAT-tailing mechanism, in cancer cells. We used GBM cells as a
304 model to conduct research, but this does not mean that these phenomena only occur in GBMs.
305 They may be widely present in the occurrence and development of cancer. Here, we focused on
306 msiCAT-tail modifications on the mitochondrial protein ATP5α. In our model, due to the specific
307 function of mitochondrial ATP synthase itself, msiCAT tail-modified proteins endow GBM cells
308 with several unique properties, such as maintaining or increasing mitochondrial membrane
309 potential despite reducing ATP production, promoting the survival and migration of GBM cells,
310 and providing resistance to STS-induced apoptosis, and this last point may be related to
311 regulating the open-close state of MPTP (Fig. 6). These characteristics promote the malignancy
312 of tumor cells, thus inhibiting the RQC pathway may be used as an effective adjuvant treatment
313 to complement existing chemotherapy methods. In addition, studying the behavior of ATP
314 synthase in cancer is also of special significance. In carcinogenesis, ATP synthase is often found
315 re-localized to the plasma membrane and is known as the ectopic ATP synthase complex (eATP
316 synthase). These eATP synthases have catalytic activity and can promote the generation of ATP
317 in the extracellular environment to establish a suitable tumor microenvironment (55). eATP
318 synthase was shown to be first assembled in mitochondria and then delivered to the cell surface
319 via microtubules (46). However, what kind of ATP synthase can be delivered to the plasma
320 membrane is not clear. Studying the localization of CAT-tailed eATP synthase in the future may
321 provide us with clues.

322 It is worth noting that more than one mitochondrial protein can be CAT-tailed in cancer
323 cells. It is very likely that the multiple nuclear-genome encoded mitochondrial proteins have

324 been CAT-tailed in the similar way, and due to the different properties of these base proteins,
325 msiCAT-tailed peptides may have diverse effects on mitochondria or cells. For example, CAT-
326 tailed COX4 protein may contribute to a more significant and direct reduction in mitochondrial
327 respiratory efficacy. It may be interesting to investigate their roles separately, as the combined
328 effects of the individual defects may be key to helping us understand the observed mitochondrial
329 changes in cancer. Indeed, in a recent study, the authors found that knocking down ANKZF1
330 inhibited the progression of GBM by causing the accumulation of abnormal proteins within
331 mitochondria (29). Combined with our data, we conclude that the balance of ANKZF1
332 expression and activity is essential for cancer proliferation. Excess or deficiency may cause
333 changes in cell adaptability. A minor drawback is that in their study, the authors used a
334 mitochondrial-localized non-stopped GFP protein to induce proteostasis stress, and there was no
335 direct biochemical evidence for detecting the CAT-tailed proteins. Here, we focus on endogenous
336 proteins to analyze the impact of target proteins on mitochondria in more detail. The
337 consideration is that abundantly expressed non-physiological ectopic proteins may cause general
338 proteostasis failure and thus mask the specific functions of endogenous proteins. In addition, the
339 cell lines used in the two studies were different. GSC is a patient-derived GBM cell line with
340 more stemness, and its mitochondrial status and RQC pathway activity may be different from
341 those of the U87 or U251 cell lines. Therefore, rather than thinking that the conclusions from the
342 two studies are in conflict, it is better to say that they are complementary, and both prove the
343 importance of RQC in tumorigenesis. Our study explores the mechanistic role of RQC pathway
344 in GBM and provides new potential targets for future treatments.

345 Comprehensive analysis of how many nuclear genome-encoded mitochondrial proteins
346 are modified through the msiCAT-tailing mechanism using advanced mass spectrometry is an

347 interesting topic and deserves further study. In a recent study published in *Cell Reports*, Lv and
348 colleagues found that the cytoplasmic E3 ligase Pirh2 and the mitochondrial protease ClpXP can
349 complement the classic NEMF-ANKZF1 to degrade mitochondrial protein aggregation caused
350 by ribosome stalling (56). The elevation of ClpXP in various cancers (57) may be explained by
351 increased msiCAT-tailing products in mitochondria, and the impact of ClpXP on mitochondrial
352 RQC also depends on future research. ClpXP also regulates the levels of a variety of
353 mitochondrial proteins. In our experiments, we found that ATP5α proteins without msiCAT-tails
354 are most difficult to ectopically express; short tails (AT3) containing proteins are better, while
355 proteins with long tails (AT20) have higher expression levels and form SDS-insoluble protein
356 aggregates. This regulation may also be achieved through the degradation of ClpXP. Another
357 possibility is regulation at the transcriptional level. The peroxisome proliferator-activated
358 receptor gamma co-activator (PGC-1α) is a master regulator of mammalian mitochondrial
359 biogenesis (58). PGC-1α can bind and activate nuclear transcription factors, leading to the
360 transcription of nuclear genome-encoded mitochondrial proteins and the mitochondrial
361 transcription factor Tfam. Tfam subsequently activates transcription and replication of the
362 mitochondrial genome (59). In the future, careful examination of the mRNA levels of the
363 msiCAT-tailed targets and the binding of PCG1α and Tfam to transcriptional elements will help
364 us distinguish between these two possibilities.

365 MPTP is an ion nonselective, calcium-dependent, and multifunctional supramolecular
366 channel that penetrates both the inner membranes of mitochondria. Although the function and
367 regulation of MPTP have been widely studied, our understanding of its molecular structure has
368 remained unclear (60). Currently, multiple structural models of MPTP have been proposed: i) the
369 VDAC (voltage-dependent anion channel)/ANT (adenine nucleotide translocator)/Cyp-D

370 (cyclophilin D) model (61). However, subsequent genetic studies have shown that whether these
371 proposed proteins are structural components of MPTP is still highly controversial (62-65). ii) the
372 ATP synthase model of MPTP. In this model, dimers of ATP synthase or reconstitution of ATP
373 synthase (c-ring) may form the molecular structure of MPTP (47, 48). This hypothesis is
374 intriguing and the role of ATP synthase as a component of the pore structure has been the subject
375 of many conflicting studies yet has not yet been unequivocally confirmed. iii) the current
376 prevalent hypothesis is that ANT and ATP synthase together form a large complex (ATP
377 synthasome), and Cyp-D regulates the dynamics of ATP synthasome (66).

378 MPTP is regulated by the physiological voltage of mitochondrial membrane potential
379 (67, 68), and conversely, the opening of MPTP can also impact ion homeostasis and energy
380 metabolism in the mitochondrial matrix. In our study, two threads converge here. The msiCAT-
381 tailed ATP5α protein helps cancer cells: i) maintain a high/stable membrane potential, which can
382 desensitize MPTP induction, and ii) directly participate in MPTP assembly, thus inhibiting
383 MPTP's function. Intriguingly, MPTP is an important mediator of cell death. However, for a long
384 time, no reports have been published to clearly confirm or refute the hypothesis, that is more
385 closed (inhibition) MPTP could be an important feature of cancer cells, which can help them
386 escape drug-induced programmed cell death. Here we present evidence supporting this
387 hypothesis. In our observation, GBM cells, especially GSC cells, have a more closed MPTP than
388 control cells. And this state is directly related to the CAT-tailing modification of the ATP
389 synthase subunit. This is also consistent with evidence that genetic mutations or post-
390 translational modifications in certain ATP synthase subunits can affect MPTP activity (69, 70).

391

392 **Materials and methods**

393 ***Cell lines and cell culture conditions***

394 The human astroglia cell line SVG p12 (ATCC, cat. CRL-8621) and the human glioma cell line
395 SF268 are provide by Dr. Rongze Olivia Lu. Both cell lines were cultured in DMEM (ATCC, cat.
396 #302002) with 10% FBS (Biowest, cat. S1620-100) and penicillin/streptomycin (Gibco™, cat.
397 15140122). SF268 clones should be maintained in complete DMEM supplemented with 400
398 μg/mL G418 (Gibco, cat. 10131027). The 0.25% trypsin solution (ATCC, cat. #SM2003C) were
399 used to passage cells. The normal human astrocytes NHA E6/E7/hTERT cell line was from Dr.
400 Russell O. Pieper, UCSF Brain Tumor Research Center. Cells are cultured in ABM™ Basal
401 Medium (Lonza, cat. CC-3187) and AGM™ SingleQuots™ Supplements (Lonza, cat. CC-4123).
402 Corning™ Accutase™ Cell Detachment Solution (Corning, cat. 25058CI) were used to passage
403 cells. GSC827 cells, a patient-derived human glioma stem cell line, was from Dr. Chun-Zhang
404 Yang at NIH. The NSC, NSC26, patient-derived GSC33, GSC22, GSC99, GSC105 and GSC107
405 cell lines used in this study were kindly provided by Dr. John S Kuo at the University of Texas,
406 Austin. GSC cells were cultured in Neural basal-A Medium (Gibco, cat. #10888022) with 2%
407 B27 (Gibco, cat. #17504044), 1% N2 (Gibco, cat. #17502048), 20 ng/ml of EGF and FGF
408 (Shenandoah Biotechnology Inc. cat. PB-500-017), Antibiotic-Antimycotic (Gibco, cat.
409 #15240062) and L-Glutamine (Gibco, cat. #250300810). Cells could be cultured in both
410 spherical and attached (on Geltrex, Thermo Fisher, cat. A1413202) forms. Corning™ Accutase™
411 Cell Detachment Solution (Cornin, cat. 25058CI) were used to passage cells.

412 Cells were transfected with X-tremeGENE™ HP DNA Transfection Reagent (Sigma, cat.
413 6366244001) following the standard protocol. For single clone selection, SF268 cells were
414 treated with 800 μg/ml G418 for 5 days. The cells were then seeded into 96-well plate at a

415 density of 1/100 μL. Positive clones were verified by immunofluorescence staining and
416 immunoblotting. Cells were maintained in complete DMEM containing 400 μg/mL G418.

417

418 ***Primers, Plasmids and viruses***

419 Plasmids pcDNA3.1+/C-(K)-DYK-ATP5F1A (pATP5α control), pcDNA3.1+/C-(K)-DYK-
420 ATP5F1A-AT3 (pATP5α-AT3), pcDNA3.1+/C-(K)-DYK-AT20 (pATP5α-AT20) were generated
421 by GenScript Inc. Plasmids pCMV-5×FLAG-β-globin-control (5FBG-Ctrl) and pCMV-
422 5×FLAG-β-globin-non-stop (5FBG-nonstop) were generated by Dr. Hoshino (Nagoya City
423 University) and Dr. Inada (Tohoku University) (43).

424 Viruses (and plasmid used to generate viruses) pLV[CRISPR]-hCas9:T2A:Neo-
425 U6>Scramble[gRNA#1] (sgControl), pLV[CRISPR]-hCas9:T2A:Neo-
426 U6>hNEMF[gRNA#1579] (sgNEMF), pLV[Exp]-Bsd-EF1A>ORF_Stuffer (pLV-control),
427 pLV[Exp]-EGFP:T2A:Puro-EF1A>mCherry (pLV-control-2), pLV[Exp]-Bsd-
428 EF1A>hANKZF1[NM_001042410.2]/HA (oeANKZF1), and pLV[Exp]-mCherry/Neo-
429 EF1A>hANKZF1[NM_001042410.2] (oeANKZF1) were made by VectorBuilder Inc.

430

431 Primers (5' to 3') used for RT-PCR are:

LONP1	lonp1_forward: TGCCTTGAACCCTCTCTAC
	lonp1_reverse: TCTGCTTGATCTTCTCCTCC
mtHSP70	mthsp70_forward: ACTCCTCCATTTATCCGCC
	mthsp70_reverse: ACCTTTGCTTGTTTACCTTCC

HSP60	hsp60_forward: ACCTGCTCTTGAAATTGCC
	hsp60_reverse: CAATCCCTCTTCTCCAAACAC
ACTB	actb_forward: TGTTTGAGACCTTCAACACC
	actb_reverse: ATGTCACGCACGATTTCC

Neurosphere formation assay of GSCs

The GSC spheroids were dissociated using Accutase for 2 min. Cells were resuspended in single cell suspension and grown under non-adherent conditions. Cells were seeded in 12-well plates at a density of $0.25x10^6$ cells/well and cultured in 3 mL culture medium for 24 hours. 20 nM of anisomycin and 150 μM of temozolomide (TMZ) were added to the culture medium and treated for 96 hours. Spheroids were images under 10x objective, captured using QCapture, and analyzed with imageJ. Spheroids larger than 50 μm were counted.

Differential gene expression analysis using the public database

The raw RNA-seq data used to perform the analysis were obtained from the University of California Santa Cruz Xenabrowser (cohort: TCGA TARGET GTEx, dataset ID: TcgaTargetGtex_rsem_gene_tpm, https://xena.ucsc.edu/), and then subsets included only TCGA glioma (GBM), GTEx Brain Frontal Cortex, and GTEx Cortex samples. Differential expression analysis was conducted using the “limma” package (R version: 4.3.1). The benjamini-Horchberg method was used for multiple testing correction to control the false discovery rate (FDR). Cut-off of adjusted p-value (adj.P.Val) was set at 0.001; cut-off of the absolute fold change was set at 2 (logFC > 1).

450

451 ***Immunostaining***

452 Cells were cultured on sterile coverslips until 80% confluency. For immunostaining, cells were
453 washed with phosphate buffered saline (PBS) solution thrice. Then, 4% formaldehyde (Thermo
454 Fisher, cat. BP531-500) was applied to cells for fixation for 30 min at room temperature. After
455 fixation, cells were washed with PBS solution containing 0.25% TritonX-100 (PBSTx) (Thermo
456 Fisher, cat. T9284) thrice, and blocked with 5% normal goat serum (Jackson Immuno, cat. 005-
457 000-121) for 1 hour at room temperature. Cells were then incubated with primary antibodies
458 overnight in a humidified chamber at 4°C. The next day, cells were washed by PBSTx thrice and
459 incubated with secondary antibodies for 2 hours at room temperature. After washing, cells were
460 stained with 300 nM DAPI (Thermo Fisher, cat. 57-481-0) for 5 min at room temperature and
461 mounted in Fluoromount-G Anti-Fade solution (Southernbiotech, cat. 0100-35). Images were
462 taken using a Zeiss LSM 800 confocal microscope, 40x oil objective lens and Airyscan
463 processing. The primary antibodies used in the study were rabbit anti-ATP5a (Cell Signaling, cat.
464 #18023), mouse anti-TOMM20 (1:500, Santa Cruz, cat. 18023S), rabbit anti-MTCO2 (1:500,
465 Abclonal, cat. sc-17764). The secondary antibodies were Alexa fluor 633-, 594-, 488-conjugated
466 secondary antibodies (1: 300, Invitrogen, cat. A21071, A11036, A32732).

467

468 ***SDS-PAGE and immunoblotting***

469 Cells or isolated mitochondria were solubilized in cell lysis buffer containing 50mM Tris-HCl
470 pH 7.4, 150 mM NaCl, 10% glycerol, 1% TritonX-100, 5 mM EDTA and 1x protease inhibitor
471 (Bimake, cat. B14002). Protein concentration was measured by using the Bradford assay
472 (BioVision, cat. K813-5000-1). Samples were separated in 4-12% Tris-Glycine gel (Invitrogen,

473 cat. WXP41220BOX) and proteins were transferred to PVDF membrane (Millipore, cat.
474 ISEQ00010). The membranes were then blocked with 5% non-fat dry milk (Kroger) for 50 min
475 at room temperature and probed with primary antibodies overnight at 4°C. Membranes were
476 washed with Tris buffered saline with 0.1% Tween 20 (TBST) solution thrice and then incubated
477 with secondary antibodies for 1 hour at room temperature. Blots were detected with ECL
478 solution (PerkinElmer, cat. NEL122001EA) and imaged by Chemidoc system (BioRad). The
479 intensity of blots was further analyzed by ImageJ software. The primary antibodies used were
480 mouse anti-Actin (1:1000, Santa Cruz, cat. sc-47778), rabbit anti-NEMF (1:1000, Proteintech,
481 cat. 11840-1-AP), mouse anti-ANKZF1 (1:1000, Santa Cruz, cat. sc-398713), mouse anti-ATP5a
482 (Abcam, cat. ab14748), mouse anti-C-I30 (1:1000, Abcam, cat. ab14711), rabbit anti-COX4
483 (Abcam, cat. ab209727), mouse anti-Flag (1:1000, Sigma, cat. F1804), rabbit anti-ANT1/2
484 (1:1000, Proteintech, cat. xxx), rabbit anti-CypD (1:1000, Proteinetch, cat. 15997-1-AP). The
485 secondary antibodies used were goat anti-rabbit IgG (1: 5000, Invitrogen, cat. G21234), goat
486 anti-mouse IgG (1:5000, Invitrogen, cat. PI31430).
487

488 ***Mitochondrial isolation, Blue Native PAGE and Western blotting***

489 Cells were homogenized using Dounce homogenizer in ice-cold homogenization buffer
490 containing 210 mM mannitol (Fisher Sci, cat. AA3334236), 70 mM sucrose (Fisher Sci, cat.
491 AA36508A1), 5 mM HEPES (Fisher Sci, cat. 15630106), pH 7.12, 1 mM EGTA (Fisher Sci, cat.
492 28-071-G), and 1x protease inhibitor. The homogenate was centrifuged at 1500 g for 5 min. The
493 resultant supernatant was centrifuged at 13000 g for 17 min. The supernatant was collected as the
494 cytosol portion and the pellet as mitochondria portion was washed with homogenization buffer
495 and centrifuged at 13000 g for 10 min. For Blue Native PAGE, the mitochondria samples were

496 solubilized in 5 % digitonin (Thermo Fisher, cat. BN2006) on ice for 30 min and then
497 centrifuged at 20000 g for 30 min. The supernatant contains solubilized mitochondrial proteins
498 and mixed with 5% G-250 (GoldBio, cat. C-460-5) and 1x NativePAGE sample buffer
499 (Invitrogen, cat. BN2008) (final G-250 concentration is 25% of the digitonin concentration).
500 Mitochondrial protein concentration was measured by using Bradford assay. Samples were
501 separated in 3-12% Bis-Tris Native gel (Invitrogen, cat. BN1001BOX) and then transferred to
502 PVDF membrane. Membranes were fixed with 8% acetic acid (Thermo Fisher, cat. 9526-33),
503 and then blocked and probed with antibodies as described above for Western blotting.

504

505 ***Mitochondrial membrane potential assays***

506 Mitochondrial membrane potential of GSC cells was measured using Image-iT^{TM} TMRM
507 (Invitrogen, cat. I34361). Cells were cultured in 96-well black plate at a density of 1 x10^5 cells
508 per well overnight in incubator with 5% CO_2 at 37°C. Cells were incubated with TMRM (100
509 nM) for 30 min at 37°C. Then, cells were washed with PBS solution three times. Fluorescence
510 changes at excitation/emission of 548/574 nm were monitored with Cytation 5 plate reader
511 (BioTek). Mitochondrial membrane potential was also measured using JC-10 (AdipoGen, cat.
512 50-114-6552). Cells were cultured in 96-well black plate at a density of 5 x 10^4 cells per well
513 overnight in incubator with 5% CO_2 at 37°C. Cells were incubated with JC-10 (10 μg/ml) for 45
514 min at 37°C. Then, cells were washed with PBS solution twice. Fluorescence changes at
515 excitation/emission of 535/595 nm for JC-10 aggregates and at 485/535 nm for JC-10 monomers
516 were monitored with a Synergy 2 Reader (BioTek). Mitochondrial membrane potential was
517 quantified as the fluorescence of JC-10 aggregates/monomers (595/535 nm).

518

519 ***Oxygen Consumption Rate assay with a Seahorse analyzer***

520 The oxygen consumption rate (OCR) of cells was measured using the Seahorse Cell Mito Stress
521 Test kit following the user guide (Agilent, cat. 103010-100). Briefly, cells were cultured in
522 testing chambers at a density of 8000 cells per well overnight in incubator with 5% CO_2 at 37°C.
523 Cells were then washed with assay medium containing Seahorse XF DMEM medium (Agilent,
524 cat. 103575-100) with 1 mM pyruvate, 2 mM glutamine and 10 mM glucose twice, and
525 incubated in assay medium for 1 hour in incubator without CO_2 at 37°C. Cells were treated with
526 compounds in the order of oligomycin (1.5 μM), carbonyl cyanide-4 (trifluoromethoxy),
527 phenylhydrazone (FCCP, 1.0 μM), and Rotenone/Antimycin (0.5 μM). The OCR of cells was
528 monitored by using Seahorse XF HS Mini (Agilent).

529

530 ***Mitochondrial MPTP assay***

531 The opening of mitochondrial permeability transition pore was measured using Invitrogen™
532 Image-IT™ LIVE Mitochondrial Transition Pore Assay Kit (Invitrogen, cat. I35103). Cells were
533 cultured in 35 mm glass-bottom dishes overnight in an incubator with 5% CO_2 at 37°C. Cells
534 were washed twice with the modified Hank's Balanced Salt Solution (HBSS, Thermo Fisher, cat.
535 14025092) containing 10 mM HEPES, 2 mM L-glutamine and 0.1 mM succinate (Thermo
536 Fisher, cat. 041983.A7) and incubated with the labeling solution (1 μM Calcein, 0.2 μM
537 MitoTracker Red, 1 mM Cobalt Chloride) for 15 min at 37°C. Cells were then washed with
538 HBSS twice and imaged at excitation/emission of 494/517 nm for Calcein and at 579/599 nm for
539 MitoTracker Red by using the Zeiss confocal microscope.

540

541 ***Mitochondrial Ca^{2+} retention capacity assay***

542 The mitochondrial calcium retention capacity (CRC) was measured on a Cytation 5 reader at
543 excitation/emission of 506/592 nm using the membrane-impermeable fluorescent probe Calcium
544 green-5N (Invitrogen, cat. C3737). Isolated mitochondria samples (0.75 mg protein/mL) were
545 incubated in 1 mL swelling medium supplemented with 10 mM succinate, 1 μM Calcium green-
546 5N, and inorganic phosphate and cyclosporine A (Thermo Fisher, cat. AC457970010). One Ca^{2+}
547 addition was 1.25 nmol (1 mL volume). Only the MPTP opening in the presence of cyclosporine
548 A was induced by high amounts of added calcium (30 nmol Ca^{2+} in the last two additions). The
549 CRC value was calculated as total Ca^{2+} accumulated in the mitochondria per unit (1 mg protein).

550

551 ***MTT assay***

552 Cell proliferation was measured by using the MTT assay kit (Roche, cat. 11465007001). Cells
553 were cultured in 96-well plates at a density of 2000 cells per well overnight in an incubator with
554 5% CO_2 at 37°C. Cells were treated with MTT labeling reagent for 4 hours at 37°C. The
555 solubilization buffer was added to cells and then cells were incubated overnight at 37°C.
556 Absorbance changes of the samples at 550 nm were monitored by using a Synergy 2 Reader
557 (BioTek).

558

559 ***Wound healing assay***

560 Cells were seeded into 6-well plates and cultured for 24-48 hours to reach a confluent cell

561 monolayer. Cells were treated with serum-free medium overnight before mechanical scratching
562 (53). Images of the wounds were taken at 0, 24 and 48 hours. Wounds areas were measured by
563 using the wound healing plugin of ImageJ. Wound coverage %=100% x $[A_{t=0h}-A_{t=\Delta h}]/A_{t=0h}$
564 ($A_{t=0h}$ is the area of the wound measured immediately after scratching $t = 0h$, $A_{t=\Delta h}$ is the area of
565 the wound measured *h* hours after scratch is performed).

566

567 ***Cell migration assay***

568 Cell migration was measured by using Transwell assays (Corning, cat. CLS3422). Cells were
569 cultured in Transwell inserts at a density of 1 x 10^5 cells per well for 3 hours in an incubator at
570 37°C with 5% CO_2. The top inserts were supplemented with DMEM medium only, and the
571 bottom wells were supplemented with DMEM medium with 20% Fetal Bovine Serum. After
572 incubation, the cells on the apical side of the Transwell insert membrane were removed using a
573 cotton applicator. The cells on the bottom side of the insert were rinsed with PBS twice and fixed
574 in 70% ethanol (Thermo Fisher, cat. R40135) for 15 min at room temperature. After fixation,
575 inserts were placed into an empty well to allow the membrane to dry. Then, the insert was
576 incubated with 0.2% crystal violet (Sigma, cat. V5265) for 5 min at room temperature. The insert
577 was rinsed with water twice and images were captured by using a microscope with a 20x
578 objective. Cell numbers were quantified using ImageJ.

579

580 ***TUNEL staining***

581 The apoptosis was measured by a TUNEL assay kit (ApexBio, cat. K1134). Cells were cultured
582 on sterile cover slips until 80% confluency and washed with PBS thrice. Then, 4% formaldehyde

583 was applied to cells and fixed for at 4°C 25 min. After fixation, cells were washed with PBS
584 twice and incubated with 20 μM proteinase K (Invitrogen, cat. 25530049) for 5 min at room
585 temperature. Then, cells were rinsed with PBS thrice and incubated in 1x equilibration buffer for
586 10 min at room temperature. Cells were stained with FITC or Cy3 labeling mix for 1 hour at
587 37°C in a humidified chamber. Cells were washed by PBS thrice and stained with DAPI for 5
588 min at room temperature. Cells were mounted in Fluoromount-G Anti-Fade solution and imaged
589 at 520 nm for FITC or at 570 nm for Cy3 by using the Zeiss confocal microscope.

590

591 ***Mitochondria ATP measurement via fluorescence imaging of ATP-red***

592 BioTracker™ ATP-red dye (Millipore, cat. SCT045) is a fluorogenic indicator for ATP in
593 mitochondria (71). Cells cultured in monolayer condition were incubated in medium with 5 μM
594 ATP-red for 15 min in an incubator at 37°C with 5% CO_2. Mitochondria were also labeled with
595 incubating cells with 100 nM MitoTracker-Green (Invitrogen, cat. M7514) for 15 min to
596 normalize their mass. Before measurement, cells were washed twice with culture medium and
597 then fresh medium was added. Cells were imaged in a 37°C chamber with 5% CO_2 at
598 excitation/emission of 510/570 nm for ATP-red and at excitation/emission of 490/516 nm for
599 MitoTracker-Green by using the Zeiss confocal microscope. The ATP-red signals could be also
600 measured by a Synergy 2 Reader (BioTek).

601

602 ***Co-immunoprecipitation***

603 Cells were lysed in the buffer containing 50 mM Tris-HCl pH 7.4, 150 mM NaCl, 10% glycerol,
604 1% TritonX-100, 5 mM EDTA and 1x protease inhibitor. Soluble samples were incubated with

605 1.5 μL ATP5α antibody at 4°C with mixing overnight. 25 μL of protein A/G magnetic beads
606 (Pierce, cat. 88802) were added to the co-IP samples and incubated at 4°C with mixing
607 overnight. Samples were washed with washing buffer thrice and then applied to SDS-PAGE
608 analysis.
609

610 ***Statistics***

611 Statistical analyses were performed by using Graphpad 7.0 software. Chi-squared test and
612 unpaired student's t-test were used for comparison. $P < 0.05$ was considered significant, expect
613 in gene expression analysis (Fig. 1A). *, $P < 0.05$; **, $P < 0.01$; ***, $P < 0.001$; ****, $P <$
614 0.0001; ns, not significant. All data were expressed as means ± s.e.m.
615

Acknowledgements

We are grateful to Dr. Chunzhang Yang at National Cancer Institute and Dr. Russell O. Pieper at University of California San Francisco for cell lines. We thank Dr. Dr. Hoshino at the Nagoya City University and Dr. Inada at the Tohoku University for providing the plasmids. We also thank members of the Wu lab at Southern Methodist University and members of the Lu lab at UCSF for helps and discussions. This work was supported by the NIH (R35GM150190 to ZW), the Cancer Prevention and Research Institute of Texas (RP210068 to ZW and RL).

Author contributions

TC and BZ designed, performed the experiments, analyzed the data and wrote the manuscript. TC, BZ, ER, YW, YT, IM, and JW performed the experiments and analyzed the data. RL and ZW formed the idea, supervised the project, wrote the manuscript and provided funding.

Conflict of interest

The authors declare no competing interests.

Materials availability

Plasmids and other materials generated in this study will be available upon request from the lead contact with a completed Materials Transfer Agreement.

636 **References**

637 1. Robichaud N, et al. Translational Control in Cancer. *Cold Spring Harbor perspectives in*
638 *biology.* 2019;11(7).
639 2. Dever TE, and Green R. The elongation, termination, and recycling phases of translation
640 in eukaryotes. *Cold Spring Harbor perspectives in biology.* 2012;4(7).
641 3. Kim KQ, and Zaher HS. Canary in a coal mine: collided ribosomes as sensors of cellular
642 conditions. *Trends in biochemical sciences.* 2022;47(1).
643 4. Brandman O, et al. A ribosome-bound quality control complex triggers degradation of
644 nascent peptides and signals translation stress. *Cell.* 2012;151(5).
645 5. Juszkiewicz S, and Hegde RS. Initiation of Quality Control during Poly(A) Translation
646 Requires Site-Specific Ribosome Ubiquitination. *Molecular cell.* 2017;65(4).
647 6. Sundaramoorthy E, et al. ZNF598 and RACK1 Regulate Mammalian Ribosome-
648 Associated Quality Control Function by Mediating Regulatory 40S Ribosomal
649 Ubiquitylation. *Molecular cell.* 2017;65(4).
650 7. Hashimoto S, et al. Identification of a novel trigger complex that facilitates ribosome-
651 associated quality control in mammalian cells. *Scientific reports.* 2020;10(1).
652 8. Juszkiewicz S, et al. The ASC-1 Complex Disassembles Collided Ribosomes. *Molecular*
653 *cell.* 2020;79(4).
654 9. Shao S, and Hegde RS. Reconstitution of a minimal ribosome-associated ubiquitination
655 pathway with purified factors. *Molecular cell.* 2014;55(6).
656 10. Shen PS, et al. Protein synthesis. Rqc2p and 60S ribosomal subunits mediate mRNA-
657 independent elongation of nascent chains. *Science (New York, NY).* 2015;347(6217).
658 11. Verma R, et al. Vms1 and ANKZF1 peptidyl-tRNA hydrolases release nascent chains

659 from stalled ribosomes. *Nature.* 2018;557(7705).

660 12. Kostova KK, et al. CAT-tailing as a fail-safe mechanism for efficient degradation of
661 stalled nascent polypeptides. *Science (New York, NY).* 2017;357(6349).

662 13. Lytvynenko I, et al. Alanine Tails Signal Proteolysis in Bacterial Ribosome-Associated
663 Quality Control. *Cell.* 2019;178(1).

664 14. Sitron CS, et al. Aggregation of CAT tails blocks their degradation and causes
665 proteotoxicity in S. cerevisiae. *PloS one.* 2020;15(1).

666 15. Choe YJ, et al. Failure of RQC machinery causes protein aggregation and proteotoxic
667 stress. *Nature.* 2016;531(7593).

668 16. Yonashiro R, et al. The Rqc2/Tae2 subunit of the ribosome-associated quality control
669 (RQC) complex marks ribosome-stalled nascent polypeptide chains for aggregation.
670 *eLife.* 2016;5.

671 17. Wu Z, et al. MISTERMINATE Mechanistically Links Mitochondrial Dysfunction With
672 Proteostasis Failure. *Molecular cell.* 2019;75(4).

673 18. Li S, et al. Quality-control mechanisms targeting translationally stalled and C-terminally
674 extended poly(GR) associated with ALS/FTD. *Proc Natl Acad Sci U S A.*
675 2020;117(40):25104-15.

676 19. Rimal S, et al. Inefficient quality control of ribosome stalling during APP synthesis
677 generates CAT-tailed species that precipitate hallmarks of Alzheimer's disease. *Acta*
678 *neuropathologica communications.* 2021;9(1).

679 20. Wang N, and Wang D. Genome-wide transcriptome and translatome analyses reveal the
680 role of protein extension and domestication in liver cancer oncogenesis. *Molecular*
681 *genetics and genomics : MGG.* 2021;296(3).

682 21. Champagne J, et al. Oncogene-dependent sloppiness in mRNA translation. *Molecular*
683 *cell.* 2021;81(22).
684 22. Rubio A, et al. Ribosome profiling reveals ribosome stalling on tryptophan codons and
685 ribosome queuing upon oxidative stress in fission yeast. *Nucleic acids research.*
686 2021;49(1).
687 23. Dango S, et al. DNA unwinding by ASCC3 helicase is coupled to ALKBH3-dependent
688 DNA alkylation repair and cancer cell proliferation. *Molecular cell.* 2011;44(3).
689 24. Gao J, et al. Suppression of ABCE1-Mediated mRNA Translation Limits N-MYC-Driven
690 Cancer Progression. *Cancer research.* 2020;80(17).
691 25. Zhou X, et al. High ANKZF1 expression is associated with poor overall survival and
692 recurrence-free survival in colon cancer. *Future oncology (London, England).*
693 2019;15(18).
694 26. Costantini S, et al. Valosin-Containing Protein (VCP)/p97: A Prognostic Biomarker and
695 Therapeutic Target in Cancer. *International journal of molecular sciences.* 2021;22(18).
696 27. Bi X, et al. Drosophila caliban, a nuclear export mediator, can function as a tumor
697 suppressor in human lung cancer cells. *Oncogene.* 2005;24(56).
698 28. Yang Q, and Gupta R. Zinc finger protein 598 inhibits cell survival by promoting UV-
699 induced apoptosis. *Oncotarget.* 2017;9(5).
700 29. Li G, et al. ANKZF1 knockdown inhibits glioblastoma progression by promoting
701 intramitochondrial protein aggregation through mitoRQC. *Cancer letters.* 2024.
702 30. Gehrke S, et al. PINK1 and Parkin control localized translation of respiratory chain
703 component mRNAs on mitochondria outer membrane. *Cell metabolism.* 2015;21(1).
704 31. Forrest MD. Why cancer cells have a more hyperpolarised mitochondrial membrane

705 potential and emergent prospects for therapy. *bioRxiv.* 2015.

706 32. Shi Y, et al. Gboxin is an oxidative phosphorylation inhibitor that targets glioblastoma.
707 *Nature.* 2019;567(7748).

708 33. Guièze R, et al. Mitochondrial Reprogramming Underlies Resistance to BCL-2 Inhibition
709 in Lymphoid Malignancies. *Cancer cell.* 2019;36(4).

710 34. Ramamoorthy MD, et al. Reserpine Induces Apoptosis and Cell Cycle Arrest in Hormone
711 Independent Prostate Cancer Cells through Mitochondrial Membrane Potential Failure.
712 *Anti-cancer agents in medicinal chemistry.* 2018;18(9).

713 35. Heerdt BG, et al. Growth properties of colonic tumor cells are a function of the intrinsic
714 mitochondrial membrane potential. *Cancer research.* 2006;66(3).

715 36. Zorova LD, et al. Mitochondrial membrane potential. *Analytical biochemistry.* 2018;552.

716 37. Maria A, et al. *Biochemistry, Electron Transport Chain.* StatPearls Publishing; 2020.

717 38. Liberti MV, and Locasale JW. The Warburg Effect: How Does it Benefit Cancer Cells?
718 *Trends in biochemical sciences.* 2016;41(3).

719 39. Varn FS, et al. Glioma progression is shaped by genetic evolution and microenvironment
720 interactions. *Cell.* 2022;185(12).

721 40. Rutka JT, et al. Establishment and characterization of five cell lines derived from human
722 malignant gliomas. *Acta neuropathologica.* 1987;75(1).

723 41. Kim E, et al. Phosphorylation of EZH2 activates STAT3 signaling via STAT3 methylation
724 and promotes tumorigenicity of glioblastoma stem-like cells. *Cancer cell.* 2013;23(6).

725 42. Sonoda Y, et al. Formation of intracranial tumors by genetically modified human
726 astrocytes defines four pathways critical in the development of human anaplastic
727 astrocytoma. *Cancer research.* 2001;61(13).

728 43. Saito S, et al. The Hbs1-Dom34 protein complex functions in non-stop mRNA decay in
729 mammalian cells. *The Journal of biological chemistry.* 2013;288(24).
730 44. Osuna BA, et al. In vitro analysis of RQC activities provides insights into the mechanism
731 and function of CAT tailing. *eLife.* 2017;6.
732 45. Morgenstern M, et al. Definition of a High-Confidence Mitochondrial Proteome at
733 Quantitative Scale. *Cell reports.* 2017;19(13).
734 46. Chang YW, et al. Spatial and temporal dynamics of ATP synthase from mitochondria
735 toward the cell surface. *Communications biology.* 2023;6(1).
736 47. Alavian KN, et al. An uncoupling channel within the c-subunit ring of the F1FO ATP
737 synthase is the mitochondrial permeability transition pore. *Proceedings of the National*
738 *Academy of Sciences of the United States of America.* 2014;111(29).
739 48. Giorgio V, et al. Dimers of mitochondrial ATP synthase form the permeability transition
740 pore. *Proceedings of the National Academy of Sciences of the United States of America.*
741 2013;110(15).
742 49. Bonora M, et al. Role of the c subunit of the FO ATP synthase in mitochondrial
743 permeability transition. *Cell cycle (Georgetown, Tex).* 2013;12(4).
744 50. Ichas F, et al. Mitochondria are excitable organelles capable of generating and conveying
745 electrical and calcium signals. *Cell.* 1997;89(7).
746 51. Stockert JC, et al. Tetrazolium salts and formazan products in Cell Biology: Viability
747 assessment, fluorescence imaging, and labeling perspectives. *Acta histochemica.*
748 2018;120(3).
749 52. Justus CR, et al. In vitro cell migration and invasion assays. *Journal of visualized*
750 *experiments : JoVE.* 2014(88).

751 53. Grada A, et al. Research Techniques Made Simple: Analysis of Collective Cell Migration
752 Using the Wound Healing Assay. *The Journal of investigative dermatology.* 2017;137(2).
753 54. Mashimo M, et al. The 89-kDa PARP1 cleavage fragment serves as a cytoplasmic PAR
754 carrier to induce AIF-mediated apoptosis. *The Journal of biological chemistry.* 2021;296.
755 55. Comelli M, et al. F1FO ATP Synthase Is Expressed at the Surface of Embryonic Rat
756 Heart-Derived H9c2 Cells and Is Affected by Cardiac-Like Differentiation. *Journal of*
757 *cellular biochemistry.* 2016;117(2).
758 56. Lv L, et al. NEMF-mediated Listerin-independent mitochondrial translational
759 surveillance by E3 ligase Pirh2 and mitochondrial protease ClpXP. *Cell reports.*
760 2024;43(3).
761 57. Cormio A, et al. Mitochondrial Caseinolytic Protease P: A Possible Novel Prognostic
762 Marker and Therapeutic Target in Cancer. *International journal of molecular sciences.*
763 2021;22(12).
764 58. Ventura-Clapier R, et al. Transcriptional control of mitochondrial biogenesis: the central
765 role of PGC-1alpha. *Cardiovascular research.* 2008;79(2).
766 59. Wu Z, et al. Mechanisms controlling mitochondrial biogenesis and respiration through
767 the thermogenic coactivator PGC-1. *Cell.* 1999;98(1).
768 60. Endlicher R, et al. The Mitochondrial Permeability Transition Pore-Current Knowledge
769 of Its Structure, Function, and Regulation, and Optimized Methods for Evaluating Its
770 Functional State. *Cells.* 2023;12(9).
771 61. Beutner G, et al. Complexes between porin, hexokinase, mitochondrial creatine kinase
772 and adenylate translocator display properties of the permeability transition pore.
773 Implication for regulation of permeability transition by the kinases. *Biochimica et*

774 *biophysica acta.* 1998;1368(1).
775 62. Baines CP, et al. Voltage-dependent anion channels are dispensable for mitochondrial-
776 dependent cell death. *Nature cell biology.* 2007;9(5).
777 63. Gutiérrez-Aguilar M, et al. Genetic manipulation of the cardiac mitochondrial phosphate
778 carrier does not affect permeability transition. *Journal of molecular and cellular*
779 *cardiology.* 2014;72.
780 64. Kokoszka JE, et al. The ADP/ATP translocator is not essential for the mitochondrial
781 permeability transition pore. *Nature.* 2004;427(6973).
782 65. Karch J, et al. Inhibition of mitochondrial permeability transition by deletion of the ANT
783 family and CypD. *Science advances.* 2019;5(8).
784 66. Beutner G, et al. The Mitochondrial Permeability Transition Pore and ATP Synthase.
785 *Handbook of experimental pharmacology.* 2017;240.
786 67. Petronilli V, et al. Regulation of the permeability transition pore, a voltage-dependent
787 mitochondrial channel inhibited by cyclosporin A. *Biochimica et biophysica acta.*
788 1994;1187(2).
789 68. Boyman L, et al. Dynamics of the mitochondrial permeability transition pore: Transient
790 and permanent opening events. *Archives of biochemistry and biophysics.* 2019;666.
791 69. Antoniel M, et al. The unique histidine in OSCP subunit of F-ATP synthase mediates
792 inhibition of the permeability transition pore by acidic pH. *EMBO reports.* 2018;19(2).
793 70. Carraro M, et al. The Unique Cysteine of F-ATP Synthase OSCP Subunit Participates in
794 Modulation of the Permeability Transition Pore. *Cell reports.* 2020;32(9).
795 71. Wang L, et al. A Multisite-Binding Switchable Fluorescent Probe for Monitoring
796 Mitochondrial ATP Level Fluctuation in Live Cells. *Angewandte Chemie (International*

797 *ed in English)*. 2016;55(5).

798

Figure Legends

Figure 1. Evidence for msiCAT-tailing on nuclear-encoded mitochondrial proteins in GBM cells

A. The expression levels of RQC genes changed significantly in GBM tumor tissues (N=153) and normal brain tissues (N=206). Significance was calculated by using unpaired student's t-test, #, logFC (fold change) > 1, adj.P.Val < 0.001.

B. Western blot analysis of msiCAT-tailed mitochondrial proteins and RQC factors in invasive patient-derived GSC and control NSC cells. Actin serves as the loading control. Red arrow heads indicate short CAT-tailed mitochondrial proteins. "short" and "long" represent exposure time. Red numbers represent fold changes in protein levels compared to controls (here NSC), labeling of fold changes in the figures below follows the same rule.

C. Western blot analysis of 5×FLAG-tagged β-globin reporter proteins in GBM and control cells, showing that the RQC system of GBM cells generates more CAT-tailed proteins. Actin serves as the loading control. Red numbers represent fold changes in protein levels compared to the control (left lane: NHA, no anisomycin).

D. Western blot analysis of overexpressed ATP5α-AT3 and ATP5α-AT20 in GBM and control cells. GAPDH serves as the loading control. SVG, SVG p12 cells; NHA, normal human astrocytes; SF, SF268 cells; GSC, GSC827 cells; labeling of cell lines in the figures below follows the same rule. Ctrl, empty vector; ATP5α, non-AT-tailed protein; AT3, ATP5α-AT3; AT20, ATP5α-AT20; labeling of transgenes in the figures below follows the same rule. Arrowheads from bottom to top indicate endogenous ATP5α, ATP5α-AT3, ATP5α-AT20, oligomers and aggregates of msiCAT-tailed ATP5α proteins.

821 E. Immunofluorescence staining shows that endogenous ATP5α proteins can form aggregates in
822 GBM cells. TOM20 (red) serves as the mitochondrial marker. Arrowheads in GBM cells indicate
823 aggregates composed by ATP5α. In this and subsequent figures, the scale bar is indicated in the
824 images.
825 F. Quantification of G. n=3, chi-squared test. ***, $P < 0.001$; ****, $P < 0.0001$. All data are
826 representative of at least 3 independent experiments. The total number of cells counted is
827 indicated in each column.
828

829 **Figure 2. msiCAT-tailed ATP5α proteins impair mitochondrial respiration but increase**
830 **mitochondrial membrane potential in GBM cells**
831 A. TMRM staining shows that patient-derived GSC (pGSC) cells display high mitochondrial
832 membrane potential. n=3, unpaired student's t-test. ***, $P < 0.001$; ****, $P < 0.0001$.
833 B. ATP measurement shows that patient-derived GSC (pGSC) cells has low mitochondrial ATP
834 production. n=3, unpaired student's t-test. **, $P < 0.01$; ***, $P < 0.001$.
835 C. JC-10 staining shows that genetic inhibition of msiCAT-tailing pathway reduces
836 mitochondrial membrane potential in GBM but not in NHA control cells. n=3, unpaired student's
837 t-test. ****, $P < 0.0001$; ns, not significant.
838 D. JC-10 staining shows that ectopic expression of ATP5α-AT3 and ATP5α-AT20 increases
839 mitochondrial membrane potential in GBM but not in control cells. n=3, unpaired student's t-
840 test. ****, $P < 0.0001$; ns, not significant.
841 E. BN-PAGE western blot for detecting ATP synthase assembly shows that ATP5α-AT3 is
842 incorporated into the composition of complex V, but ATP5α-AT20 forms high molecular weight

843 protein aggregates in mitochondria of GBM cells. SC: respiratory supercomplex; C-V: complex
844 V/ATP synthase.
845 F, H. OCR indicates that the reduction of mitochondrial consumption rate of SF268 cells with
846 ATP5α-AT3 and ATP5α-AT20 expression. Oligomycin (1.5 μM), FCCP (1.0 μM), and
847 rotenone/antimycin A (R/A, 0.5 μM) were added sequentially to the reaction cells.
848 G, I. Statistical summary of mitochondrial respiration parameters in F and H, including non-
849 mitochondrial respiration, basal respiration, maximum respiration, spare respiration, proton leaks
850 and ATP production. n=3, unpaired student's t-test. *, $P < 0.05$; **, $P < 0.01$; ***, $P < 0.001$;
851 ****, $P < 0.0001$; ns, not significant.
852

853 **Figure 3**. **msiCAT-tailing product regulates mPTP status in GBM cells**
854 A. Mitochondrial transition pore assay shows that GBM has reduced mPTP opening compared to
855 NHA controls, which can be reversed by transient anisomycin treatment (200 nM).
856 B. Quantification of A. n=3, unpaired student's t-test. ****, $P < 0.0001$.
857 C. Calcium retention capacity (CRC) of isolated mitochondria from cells measured by using
858 Calcium Green-5N dye. NHA is used as the control cell line. Cyclosporin A (CsA, a mPTP
859 inhibitor)-treated sample serves as a positive control.
860 D. Statistic of C. The data shows that GBM cells exhibited high CRC, whereas mitochondria
861 from cells pretreated with anisomycin (200 nM) or with NEMF knockout (sgNEMF) are
862 attenuated. n=3, unpaired student's t-test. ***, $P < 0.001$; ****, $P < 0.0001$.
863 E. Mitochondrial transition pore assay shows that ectopic expression of ATP5α-AT3 and ATP5α-
864 AT20 inhibits mPTP opening in GBM cells.
865 F. Quantification of E. n=3, unpaired student's t-test. ****, $P < 0.0001$.

866 G. BN-PAGE western blot shows that the expression of ATP5α-AT3 and ATP5α-AT20 changes
867 the pattern of ANT1/2 protein in GBM cells, missing a band (marked by a red * on the blot), and
868 forming high molecular weight protein aggregates. SC: respiratory supercomplex; C-V: complex
869 V/ATP synthase.
870

871 **Figure 4. msiCAT-tailed ATP5α protein promotes GBM progression**

872 A. MTT assay shows that the expression of ATP5α-AT3 and ATP5α-AT20 promotes GBM cell
873 proliferation. n=3, unpaired student's t-test. **, $P < 0.01$; ***, $P < 0.001$.

874 B. MTT assay shows that the expression of ATP5α-AT3 and ATP5α-AT20 does not promote
875 NHA cell proliferation. n=3, unpaired student's t-test. ns, not significant.

876 C. Transwell assay shows that the expression of ATP5α-AT3 and ATP5α-AT20 promotes GBM
877 cell (SF) but not control cell (NHA) migration.

878 D. Quantification of C showing the number of migrated cells. n=3, unpaired student's t-test.
879 ****, $P < 0.0001$; ns, not significant.

880 E. TUNEL staining shows that the expression of ATP5α-AT3 and ATP5α-AT20 can block STS (1
881 μM)-induced apoptosis in GBM cells. TUNEL-Cy3 was used to indicate apoptotic cells. DAPI
882 was used to stain nucleus.

883 F. Quantification of E showing the percentage of TUNEL-positive cells in the population. n=3,
884 unpaired student's t-test. ****, $P < 0.0001$.

885 G. MTT assay shows that the expression of ATP5α-AT3 and ATP5α-AT20 enhances resistance to
886 temozolomide (TMZ, 150 μM). TMZ treated SF-Ctrl group is used as the control. n=3, unpaired
887 student's t-test. ***, $P < 0.001$.
888

889 **Figure 5. Inhibition of msiCAT-tailing impedes GBM progression**

890 A. Cell viability assay shows that patient-derived GSC (pGSC) cells are significantly lower than
891 control NSC cells, after 48 hours of anisomycin treatment. ***, $P < 0.001$; ****, $P < 0.0001$,
892 compared to the NSC controls at a certain dose of anisomycin.

893 B. Cell viability assay shows that genetic inhibition of msiCAT-tailing pathway hampers GBM
894 cell proliferation. **, $P < 0.01$; ***, $P < 0.001$; ****, $P < 0.0001$, compared to the control group
895 at the corresponding time.

896 C. Transwell assay shows that genetic inhibition of msiCAT-tailing pathway blocks GBM cell
897 (SF) but not control cell (NHA) migration.

898 D. Quantification of C showing the number of migrated cells. n=3, unpaired student's t-test. ***,
899 $P < 0.001$; ns, not significant.

900 E. JC-10 staining shows that pharmacological inhibition of msiCAT-tailing synthesis with
901 anisomycin reduces mitochondrial membrane potential in GBM but not in NHA control cells.
902 n=3, unpaired student's t-test. ***, $P < 0.001$; ns, not significant.

903 F. Western blot analysis of PARP in anisomycin treated and untreated GSC cells shows that
904 pharmacological inhibition of msiCAT-tailing pathway potentiates STS-induced apoptosis.
905 Red numbers below the blots represent the ratio of cleaved PARP (c-PARP) to PARP protein.
906 Actin serves as the loading control.

907 G. TUNEL staining shows that pharmacological inhibition of msiCAT-tailing pathway promotes
908 STS (1 μM)-induced apoptosis in GBM cells. TUNEL-Cy3 is used to indicate apoptotic cells.
909 DAPI is used to stain nucleus.

910 H. Quantification of G showing the percentage of TUNEL-positive cells in the population. n=3,
911 unpaired student's t-test. **** $P < 0.0001$. DMSO is used as the vehicle control.

912 I. Cell viability assay shows that pharmacological inhibition of msiCAT-tailing pathway could
913 reduce the resistance of GBM cells to TMZ treatment (150 μM). n=3, unpaired student's t-test. *
914 $P < 0.05$; **, $P < 0.01$.
915 J. Neurosphere formation assay shows that pharmacological inhibition of msiCAT-tailing
916 pathway can cooperate with TMZ to reduce the formation of spheroids in GBM cells, indicating
917 the reduction of drug resistance.
918 K. Quantification of J. n=3, unpaired student's t-test. **, $P < 0.01$.
919

920 **Figure 6. A working model of how msiCAT-tail modified ATP5α protein affects**
921 **mitochondrial function in GBM cells**
922 In normal cells, the ATP5α protein encoded by the nuclear genome enters the mitochondrial
923 matrix through a co-translational import mechanism through the TOM/TIM complex and is
924 subsequently assembled into ATP synthase (Left Side). In GBM cells, the CAT-tailed ATP5α
925 protein forms insoluble aggregates close to the outer membrane of mitochondria or can be
926 imported into mitochondria. In the mitochondrial matrix, proteins with shorter CAT-tails easily
927 incorporate into ATP synthase and affect its function, which is manifested by a decrease in the
928 ATP synthesis rate and accumulation of protons (H^+), resulting in an increase in mitochondrial
929 membrane potential. Ultimately, changes in ATP synthase leads to the malfunction of mPTP,
930 thereby affecting cell proliferation, migration and resistance to drug-induced apoptosis (Right
931 Side).

932

933 **Supplementary Figure and Table Legends**

934 **Figure S1. The RQC pathway is disturbed in GBM cells**

935 A. Western blot analysis of some RQC factors in control (SVG, NHA) and GBM (SF268,
936 GSC827) cell lines. Actin serves as the loading control. Red * indicates a modified form of
937 NEMF in GSC827 cells. Red numbers represent fold changes in protein levels compared to
938 controls (here SVG), labeling of fold changes in the figures below follows the same rule.

939 B. Immunofluorescence staining shows that Flag-tagged ATP5α-AT3 and ATP5α-AT20 (green)
940 form aggregates in GBM and control cells. TOM20 (red) serves as the mitochondrial marker. In
941 this and subsequent figures, the scale bar is indicated in the images.

942 C. Quantification of A, n=3, chi-squared test. ****, $P < 0.0001$. The total number of cells
943 counted is indicated in each column.

944

945 **Table S1. Differential expression analysis for RQC genes in GBM patients and healthy**
946 **controls**

947

948 **Figure S2. GBM cells have high mitochondrial membrane potentials but low mitochondrial**
949 **ATP levels**

950 A. JC-10 staining shows that GBM cells have high mitochondrial membrane potentials than
951 NHA (control) cells. n=3, unpaired student's t-test. ***, $P < 0.001$

952 B. BioTracker ATP-red dye staining shows that GBM cells have low mitochondrial ATP
953 production than NHA (control) cells. MitoTracker Green is used to indicate mitochondrial mass.

954 C. Quantification of B. n=3, unpaired student's t-test. ****, $P < 0.0001$.

D. Western blot analysis shows the efficiency of overexpression and knockdown in cells. Actin serves as the loading control.

Figure S3. The regulation of mPTP by CAT-tailing on ATP5α

A. Immunofluorescence staining shows that anisomycin (200 nM) treatment inhibits protein aggregation formed by endogenous ATP5α. TOM20 (red) serves as the mitochondrial marker.

B. Quantification of A, n=3, chi-squared test. *, $P < 0.05$. The total number of cells counted is indicated in each column.

C. Co-immunoprecipitation shows no direct interaction between ATP5α and CypD or ANT1/2 can be found in GBM cells. Red arrowheads indicate target proteins.

D. Western blotting of cytosolic and isolated mitochondrial samples shows that expression of ATP5α-AT3 reduces CypD levels in GBM cells. TOM20 serves as the mitochondrial marker and loading control.

Figure S4. msiCAT-tailing regulates cell survival in GBM cells

A. Wound healing assay shows that the expression of ATP5α-AT3 and ATP5α-AT20 promotes GBM cell (SF268) migration.

B. Quantification of A showing the healing rate indicated by scratch wound coverage after 24 and 48 hours. n=3, unpaired student's t-test. **, $P < 0.01$.

C. RT-PCR shows no significant increase of mitochondrial unfolded protein response markers. Actin serves as the loading control.

D. TUNEL staining shows that GBM cells are more resistant to STS (1 μM)-induced apoptosis than control cells. TUNEL-Cy3 is used to indicate apoptotic cells. DAPI is used to stain nucleus.

E. Quantification of C showing the percentage of TUNEL-positive cells in the population. n=3, unpaired student's t-test. ***, $P < 0.0001$; ****, $P < 0.0001$.

F. Western blot analysis of PARP shows that GBM cells are more resistant to apoptosis induced by 30, 90, 180 min of STS (1 μM) treatment. Cleaved PARP serves as an indicator for apoptosis. Actin and GAPDH are used as loading controls. Red numbers below the blots represent the ratio of cleaved PARP (c-PARP) to PARP protein.

Figure S5. Inhibition of msiCAT-tailing promotes apoptosis

A. Cell viability assay shows that genetic inhibition of msiCAT-tailing pathway also hampers NHA cell proliferation. **, $P < 0.01$; ****, $P < 0.0001$, compared to the control group at the corresponding time.

B. Transwell assay shows that pharmacological inhibition of msiCAT-tailing pathway blocks GSC cell (SF) but not control cell (NHA) migration.

C. Quantification of C showing the number of migrated cells. n=3, unpaired student's t-test. ****, $P < 0.0001$; ns, not significant.

D. TUNEL staining shows that genetic inhibition of msiCAT-tailing pathway promotes STS (1 μM)-induced apoptosis in GBM cells. TUNEL-FITC is used to indicate apoptotic cells. DAPI is used to stain nucleus.

E. Quantification of G showing the percentage of TUNEL-positive cells in the population. n=3, unpaired student's t-test. **** $P < 0.0001$. DMSO is used as the vehicle control.

Figure 1

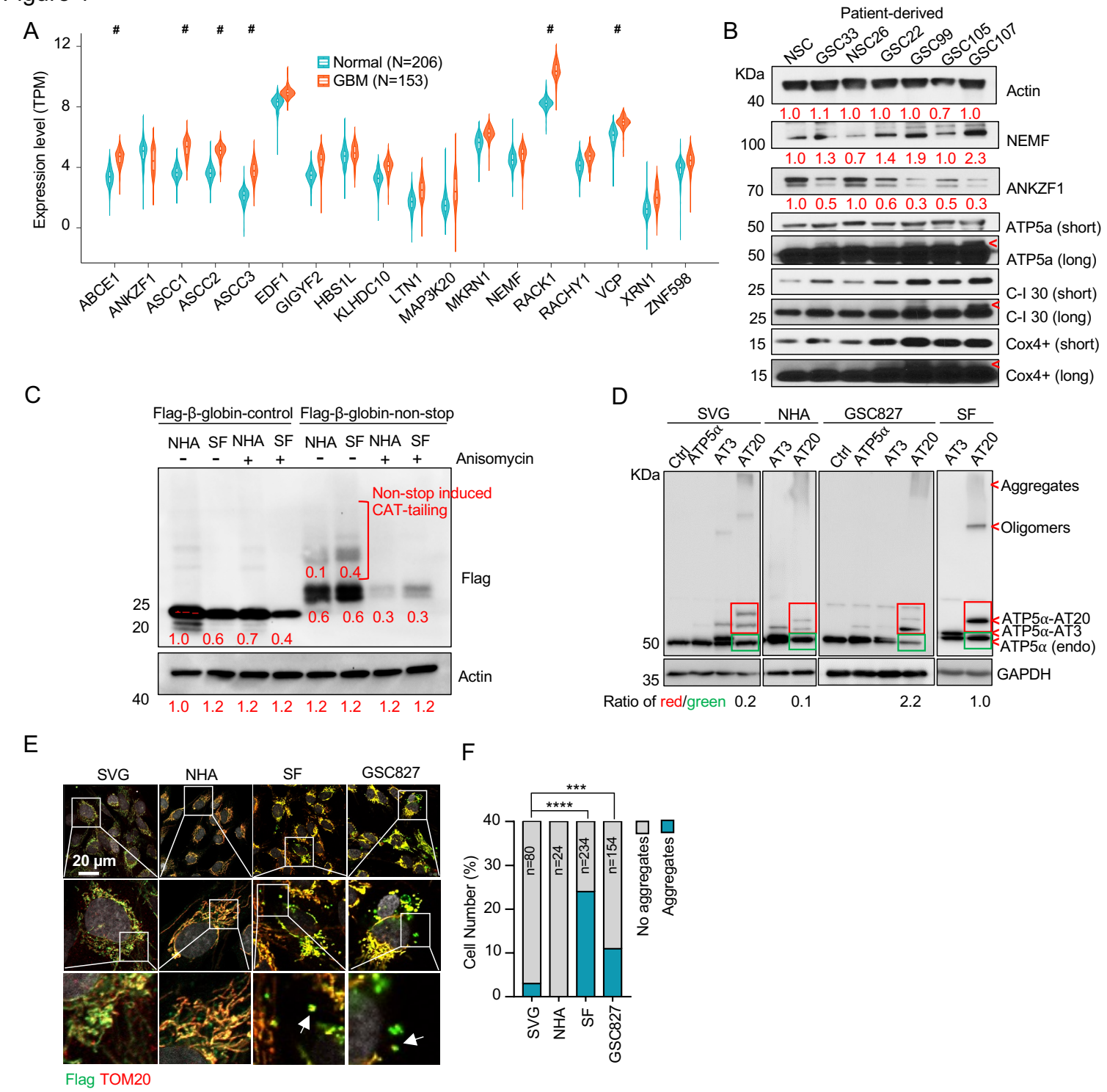
A
Normal (N=206)
GBM (N=153)
Expression level (TPM)
ABCE1
ANKZF1
ASCC1
ASCC2
ASCC3
EDF1
GIGYF2
HBS1L
KLHDC10
LTN1
MAP3K20
MKRN1
NEMF
RACK1
RACHY1
VCP
XRN1
ZNF598
B
Patient-derived
NSC
GSC33
NSC26
GSC22
GSC99
GSC105
GSC107
KDa
Actin
NEMF
ANKZF1
ATP5a (short)
ATP5a (long)
C-I 30 (short)
C-I 30 (long)
Cox4+ (short)
Cox4+ (long)
C
Flag-β-globin-control
Flag-β-globin-non-stop
NHA SF NHA SF NHA SF NHA SF
Anisomycin
Non-stop induced
CAT-tailing
Flag
Actin
D
SVG
NHA
GSC827
SF
Ctrl
ATP5α
AT3
AT20
KDa
Aggregates
Oligomers
ATP5α-AT20
ATP5α-AT3
ATP5α (endo)
GAPDH
Ratio of red/green 0.2 0.1 2.2 1.0
E
SVG
NHA
SF
GSC827
20 μm
Flag TOM20
F
Cell Number (%)
No aggregates
Aggregates
n=80
n=24
n=234
n=154
SVG
NHA
SF
GSC827

Figure 2

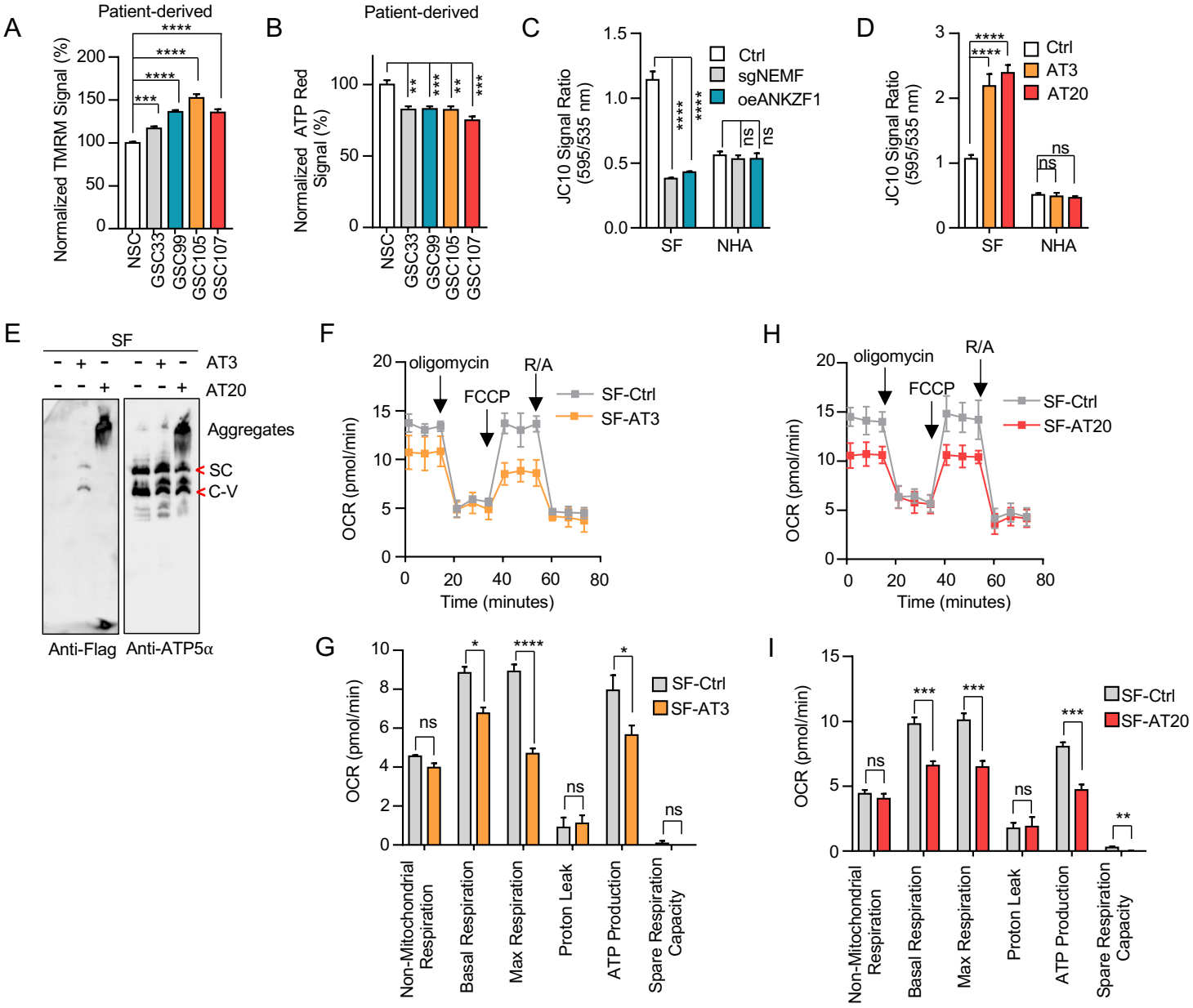
A
Patient-derived
Normalized TMRM Signal (%)
NSC
GSC33
GSC99
GSC105
GSC107
B
Patient-derived
Normalized ATP Red Signal (%)
C
JC10 Signal Ratio (595/535 nm)
Ctrl
sgNEMF
oeANKZF1
SF
NHA
D
JC10 Signal Ratio (595/535 nm)
Ctrl
AT3
AT20
E
SF
AT3
AT20
Aggregates
SC
C-V
Anti-Flag
Anti-ATP5α
F
oligomycin
FCCP
R/A
SF-Ctrl
SF-AT3
OCR (pmol/min)
Time (minutes)
H
oligomycin
FCCP
R/A
SF-Ctrl
SF-AT20
OCR (pmol/min)
Time (minutes)
G
OCR (pmol/min)
SF-Ctrl
SF-AT3
Non-Mitochondrial Respiration
Basal Respiration
Max Respiration
Proton Leak
ATP Production
Spare Respiration Capacity
I
OCR (pmol/min)
SF-Ctrl
SF-AT20
Non-Mitochondrial Respiration
Basal Respiration
Max Respiration
Proton Leak
ATP Production
Spare Respiration Capacity

Figure 3

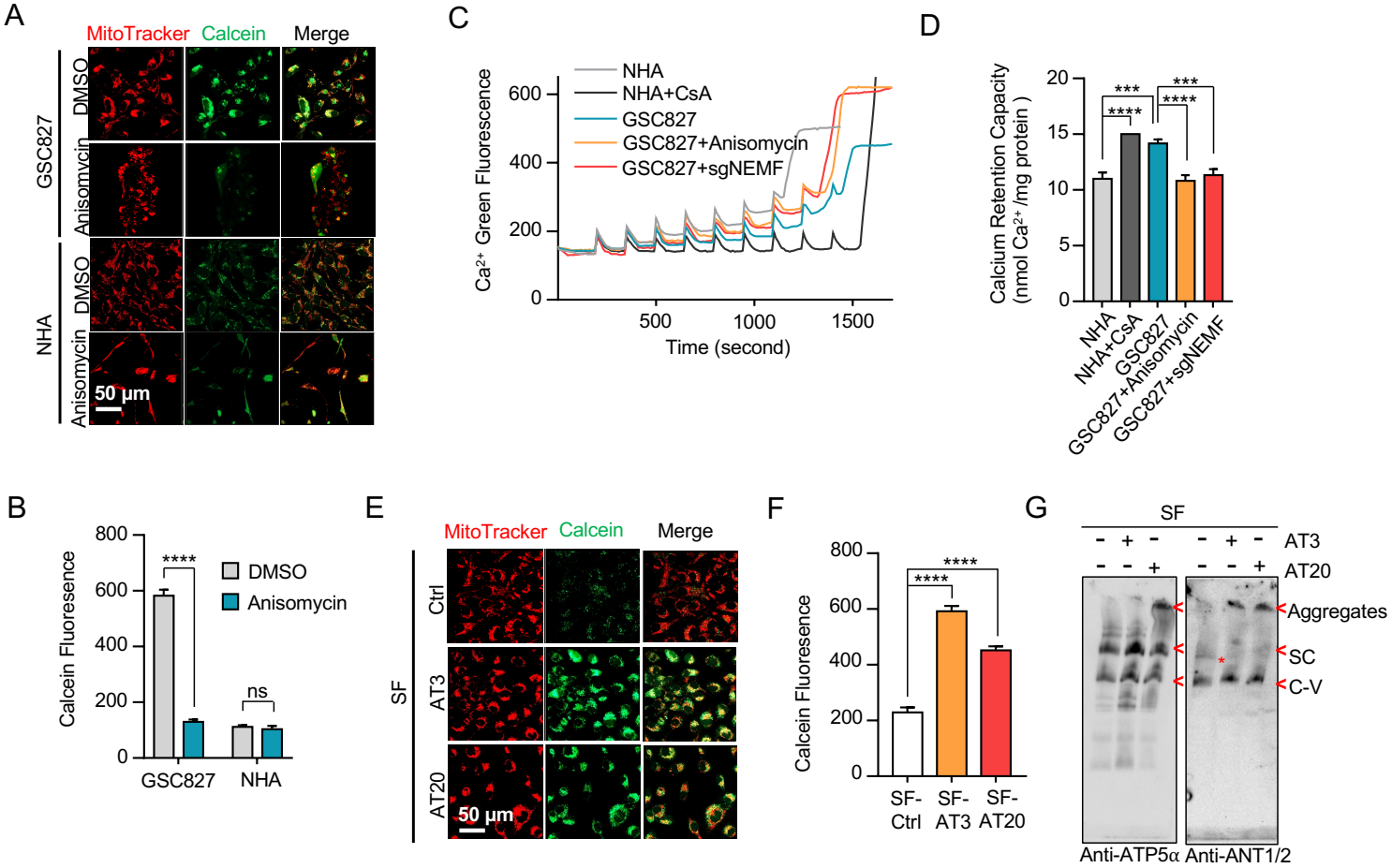
A
MitoTracker
Calcein
Merge
GSC827
DMSO
Anisomycin
NHA
DMSO
Anisomycin
50 μm
C
NHA
NHA+CsA
GSC827
GSC827+Anisomycin
GSC827+sgNEMF
Ca2+ Green Fluorescence
600
400
200
0
500
1000
1500
Time (second)
D
Calcium Retention Capacity
(nmol Ca2+ /mg protein)
20
15
10
5
0
***
****
***
****
NHA
NHA+CsA
GSC827
GSC827+Anisomycin
GSC827+sgNEMF
B
Calcein Fluoresence
800
600
400
200
0
****
ns
DMSO
Anisomycin
GSC827
NHA
E
MitoTracker
Calcein
Merge
SF
Ctrl
AT3
AT20
50 μm
F
Calcein Fluoresence
800
600
400
200
0
****
****
SF-Ctrl
SF-AT3
SF-AT20
G
SF
AT3
AT20
Aggregates
SC
C-V
Anti-ATP5α
Anti-ANT1/2

Figure 4

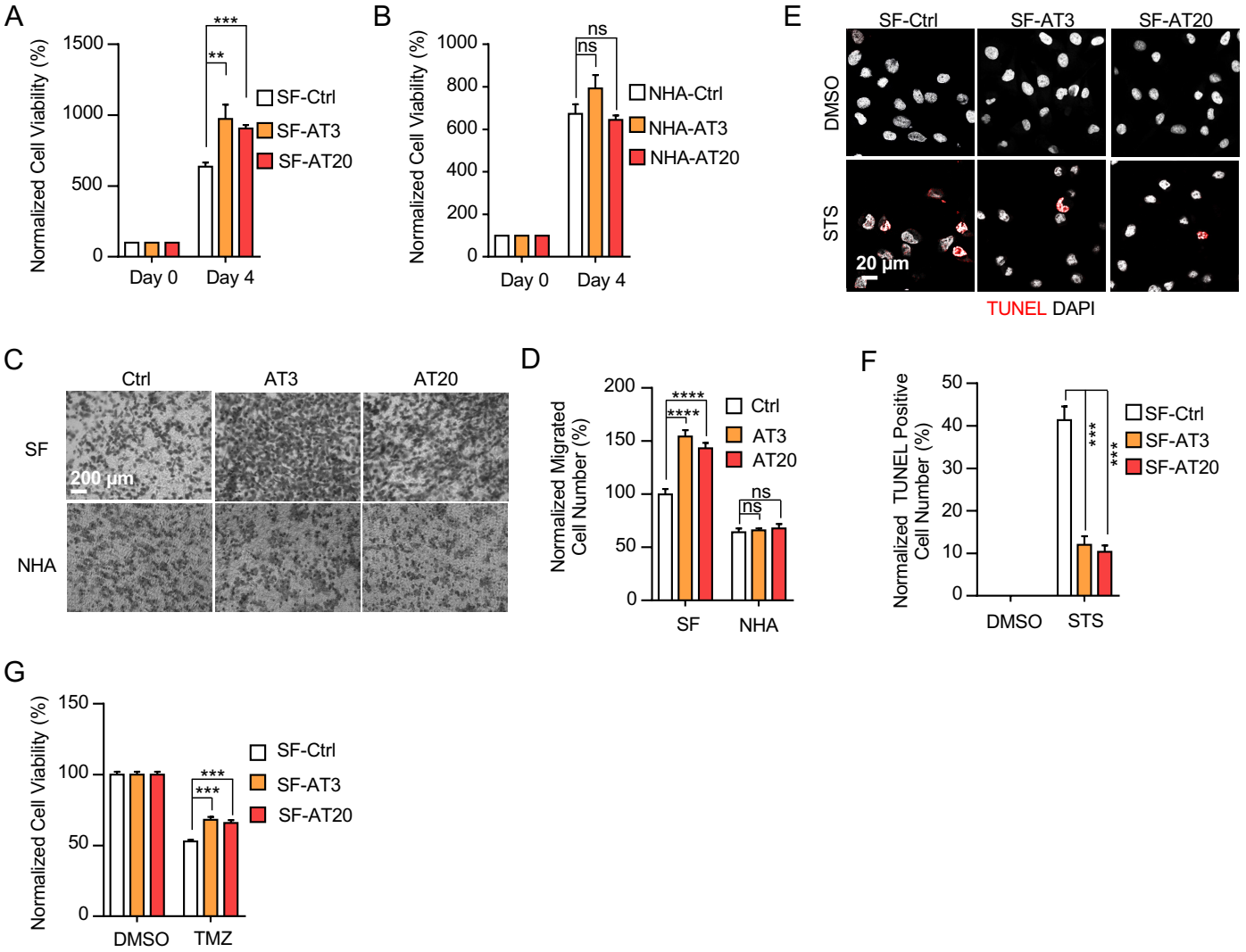
A
Normalized Cell Viability (%)
1500
1000
500
0
Day 0
Day 4
***
**
SF-Ctrl
SF-AT3
SF-AT20
B
Normalized Cell Viability (%)
1000
800
600
400
200
0
Day 0
Day 4
ns
ns
NHA-Ctrl
NHA-AT3
NHA-AT20
E
SF-Ctrl
SF-AT3
SF-AT20
DMSO
STS
20 µm
TUNEL DAPI
C
Ctrl
AT3
AT20
SF
NHA
200 µm
D
Normalized Migrated Cell Number (%)
200
150
100
50
0
****
****
ns
ns
Ctrl
AT3
AT20
SF
NHA
F
Normalized TUNEL Positive Cell Number (%)
50
40
30
20
10
0
***
***
SF-Ctrl
SF-AT3
SF-AT20
DMSO
STS
G
Normalized Cell Viability (%)
150
100
50
0
***
***
SF-Ctrl
SF-AT3
SF-AT20
DMSO
TMZ

Figure 5

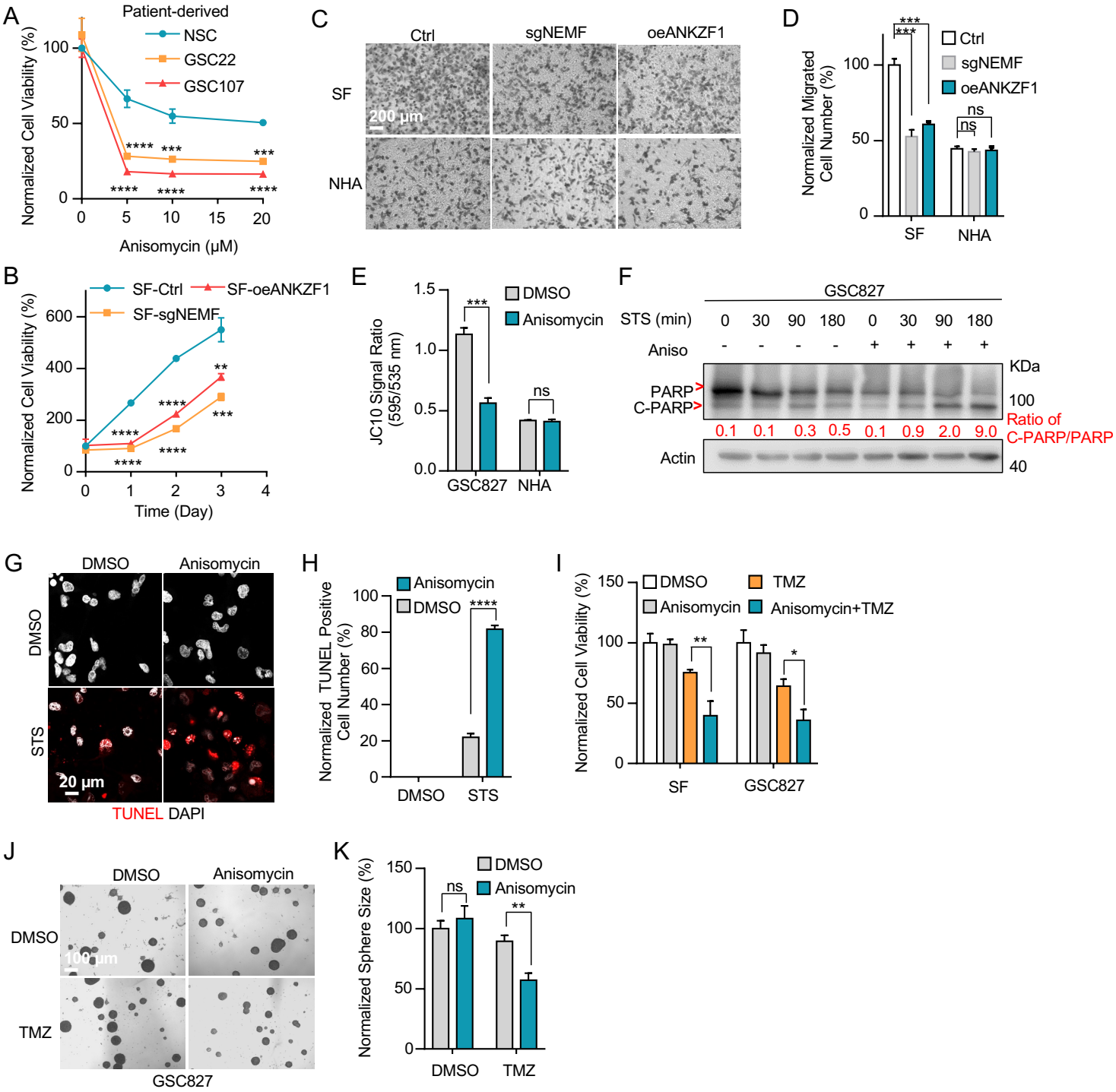
A
Patient-derived
NSC
GSC22
GSC107
Normalized Cell Viability (%)
Anisomycin (μM)
B
SF-Ctrl
SF-oeANKZF1
SF-sgNEMF
Normalized Cell Viability (%)
Time (Day)
C
Ctrl
sgNEMF
oeANKZF1
SF
NHA
200 μm
D
Ctrl
sgNEMF
oeANKZF1
Normalized Migrated Cell Number (%)
SF
NHA
E
DMSO
Anisomycin
JC10 Signal Ratio (595/535 nm)
GSC827
NHA
F
GSC827
STS (min)
Aniso
KDa
PARP
C-PARP
Ratio of C-PARP/PARP
Actin
G
DMSO
Anisomycin
STS
20 μm
TUNEL DAPI
H
Anisomycin
DMSO
Normalized TUNEL Positive Cell Number (%)
DMSO
STS
I
DMSO
TMZ
Anisomycin
Anisomycin+TMZ
Normalized Cell Viability (%)
SF
GSC827
J
DMSO
Anisomycin
TMZ
100 μm
GSC827
K
DMSO
Anisomycin
Normalized Sphere Size (%)
DMSO
TMZ

Figure 6

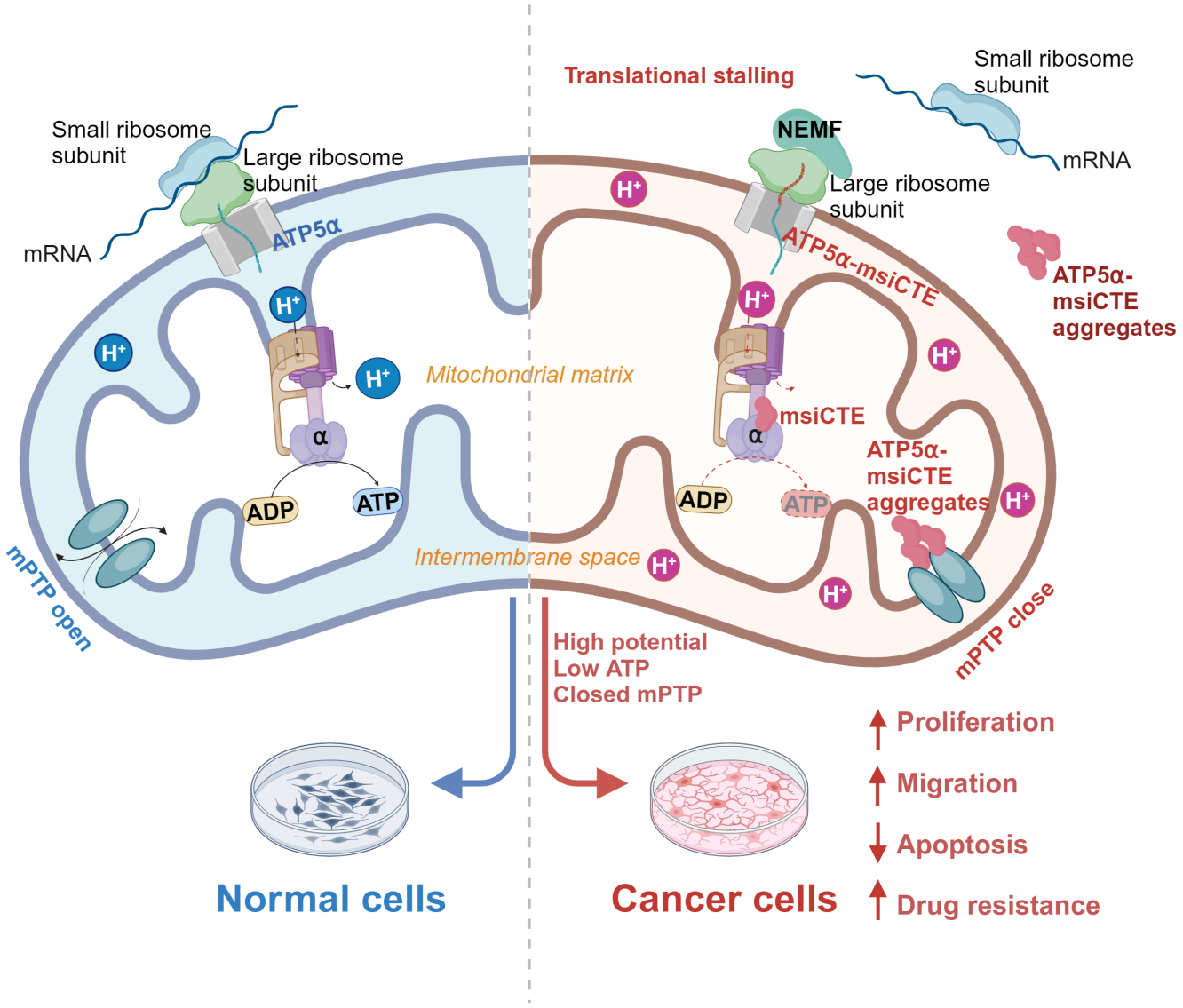

Created with BioRender.com
By Bei Zhang

Figure S1

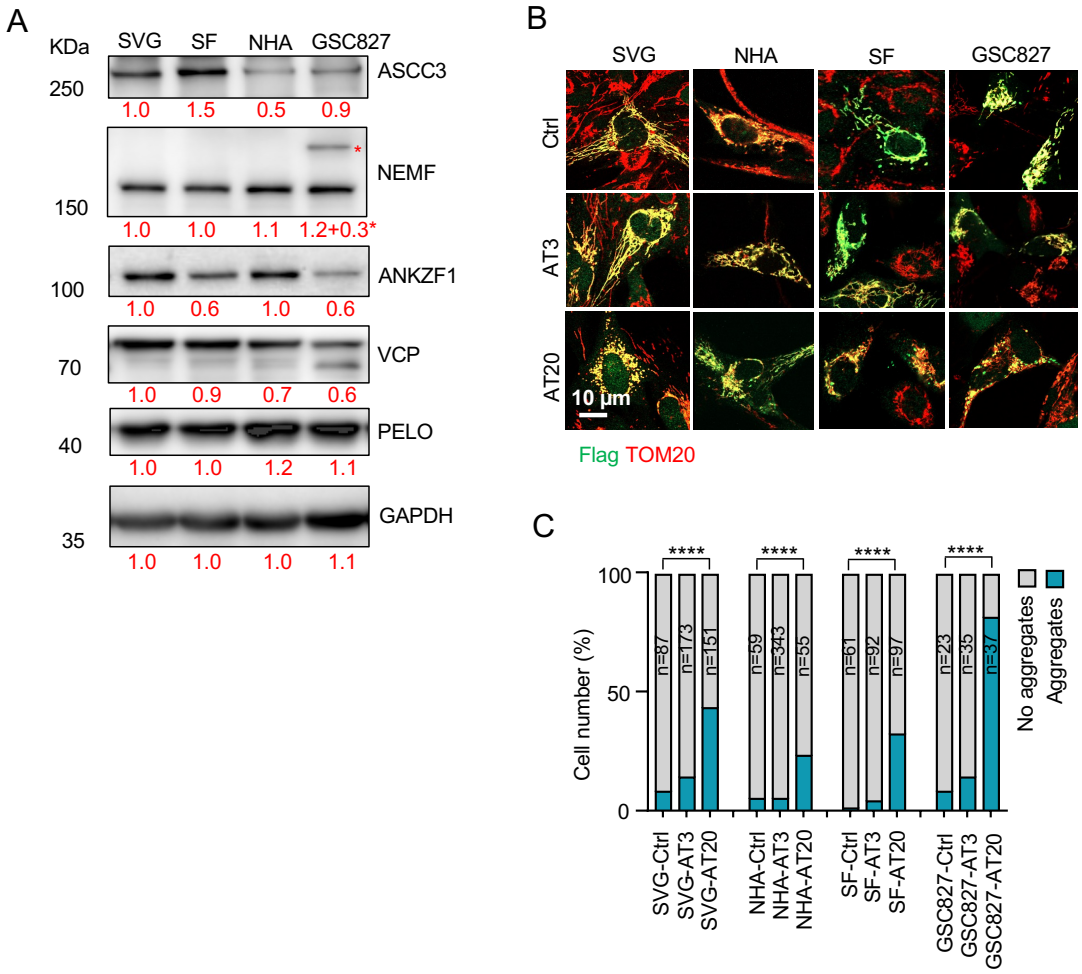
A
KDa
SVG
SF
NHA
GSC827
250
ASCC3
1.0 1.5 0.5 0.9
150
NEMF
*
1.0 1.0 1.1 1.2+0.3*
100
ANKZF1
1.0 0.6 1.0 0.6
70
VCP
1.0 0.9 0.7 0.6
40
PELO
1.0 1.0 1.2 1.1
35
GAPDH
1.0 1.0 1.0 1.1
B
SVG
NHA
SF
GSC827
Ctrl
AT3
AT20
10 µm
Flag TOM20
C
Cell number (%)
100
50
0
****
n=87
n=173
n=151
n=59
n=343
n=55
n=61
n=92
n=97
n=23
n=35
n=37
SVG-Ctrl
SVG-AT3
SVG-AT20
NHA-Ctrl
NHA-AT3
NHA-AT20
SF-Ctrl
SF-AT3
SF-AT20
GSC827-Ctrl
GSC827-AT3
GSC827-AT20
No aggregates
Aggregates

Table S1

Table S1. Differential expression analysis for RQC genes in GBM patients and healthy controls

Gene	logFC	AveExpr	t	P.Value	adj.P.Val
RACK1	2.224548565	9.048113333	19.24641934	2.62E-57	6.69E-56
ASCC3	1.738216567	2.717246389	19.27211713	2.05E-57	5.27E-56
ASCC1	1.689584768	4.257915556	17.8774401	1.20E-51	2.18E-50
ASCC2	1.471467207	4.153399167	15.9118075	1.43E-43	1.68E-42
ABCE1	1.32826428	3.81695	13.79248369	4.69E-35	3.60E-34
VCP	1.050066326	6.321021667	9.828944092	2.33E-20	9.31E-20
GIGYF2	0.985695112	3.786421389	10.25440005	8.00E-22	3.41E-21
MAP3K20	0.962218073	1.863793889	8.711292467	1.10E-16	3.75E-16
PELO	0.92860628	2.2885625	10.60122263	4.85E-23	2.18E-22
KLHDC10	0.854921284	3.492322222	9.064976509	8.08E-18	2.88E-17
EDF1	0.82091202	8.444505	7.278600017	2.12E-12	5.94E-12
XRN1	0.809119864	1.518371111	8.54020086	3.80E-16	1.26E-15
LTN1	0.786409776	1.9716	9.962815742	8.14E-21	3.32E-20
MKRN1	0.769369764	5.745359444	7.400071791	9.65E-13	2.74E-12
RCHY1	0.652647968	4.276126111	6.840213538	3.40E-11	8.93E-11
ZNF598	0.62380412	4.006663611	6.043582081	3.76E-09	8.90E-09
HBS1L	0.291107388	4.701389722	2.72853772	0.006672805	0.010370549
NEMF	0.194631373	4.566962778	2.575063266	0.010419695	0.015855894
ANKZF1	-0.436070986	4.620298333	-3.65005718	0.000300886	0.000525859

Abbreviations: RQC, ribosome-associated quality control; GBM, glioblastoma.

Figure S2

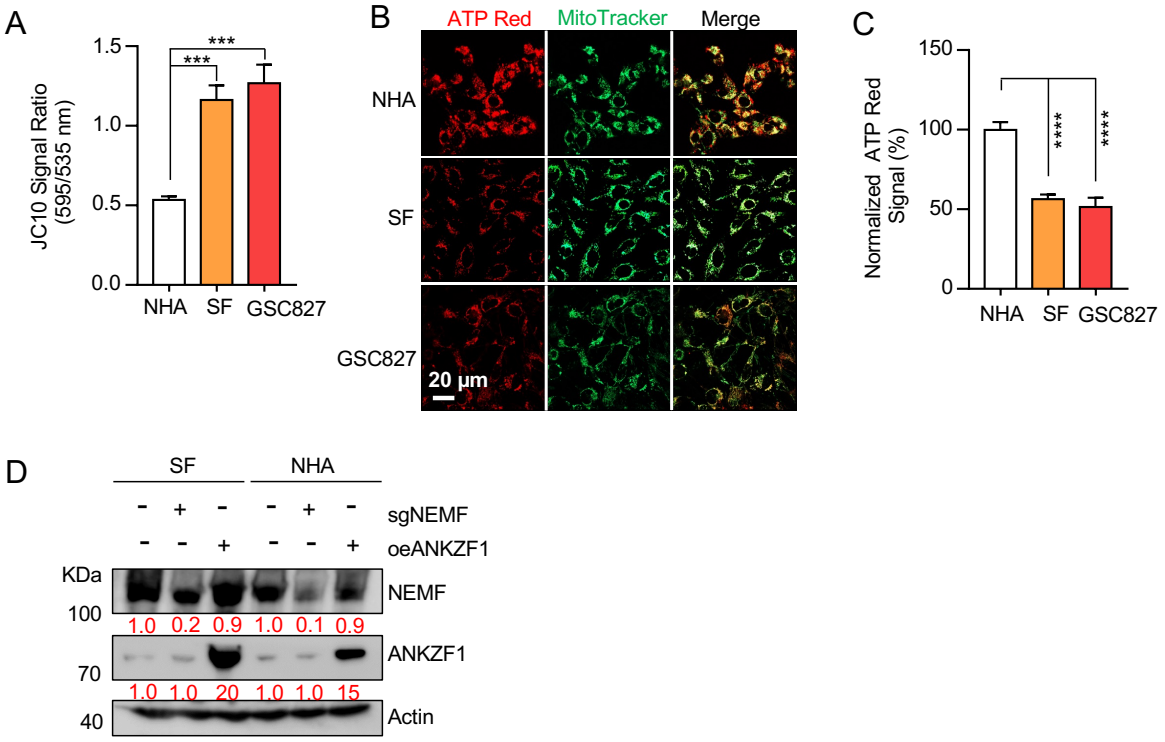
A
JC10 Signal Ratio (595/535 nm)
1.5
1.0
0.5
0.0
***
***
NHA
SF
GSC827
B
ATP Red
MitoTracker
Merge
NHA
SF
GSC827
20 μm
C
Normalized ATP Red Signal (%)
150
100
50
0
****
****
NHA
SF
GSC827
D
SF
NHA
sgNEMF
oeANKZF1
KDa
100
70
40
NEMF
ANKZF1
Actin
1.0 0.2 0.9 1.0 0.1 0.9
1.0 1.0 20 1.0 1.0 15

Figure S3

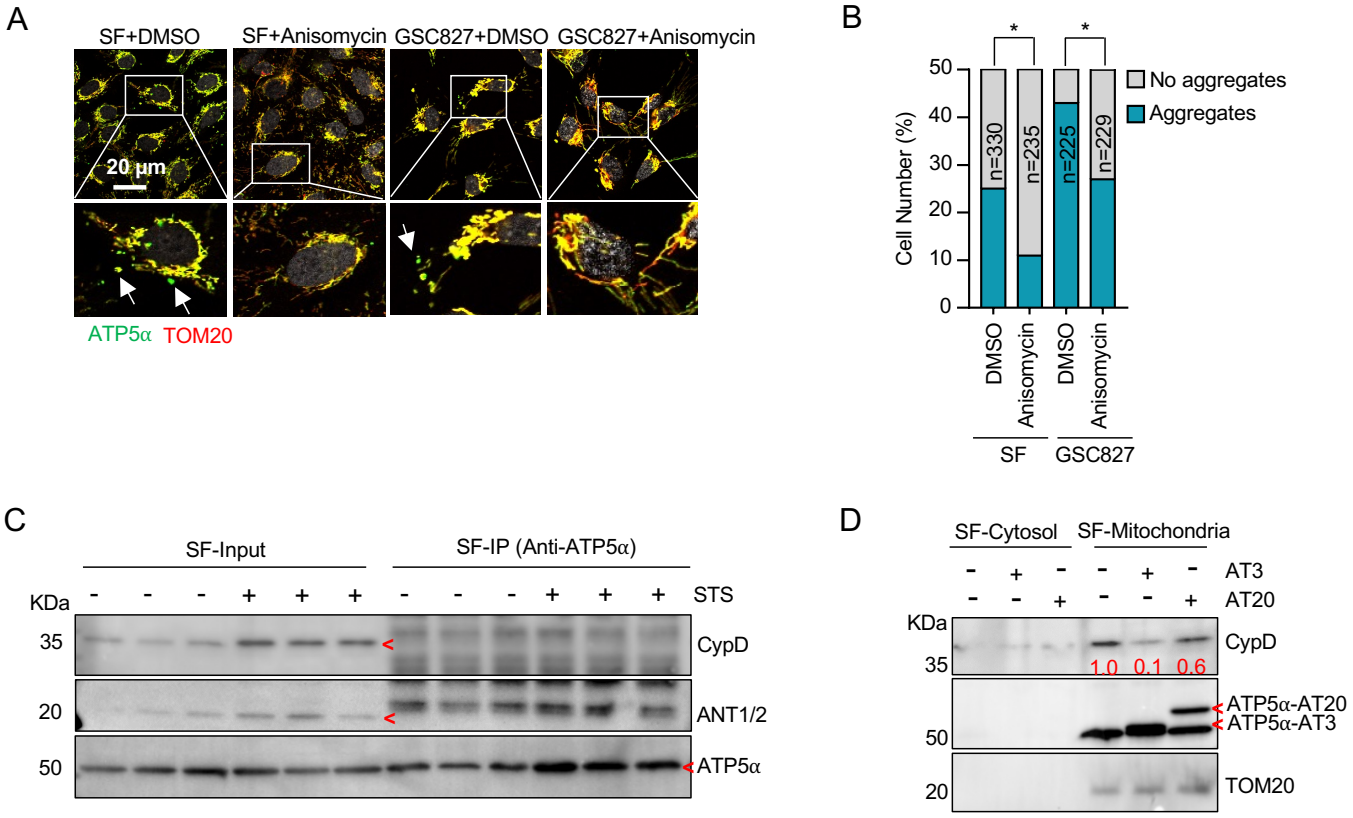
A
SF+DMSO
SF+Anisomycin
GSC827+DMSO
GSC827+Anisomycin
20 μm
ATP5α
TOM20
B
Cell Number (%)
No aggregates
Aggregates
n=330
n=235
n=225
n=229
DMSO
Anisomycin
DMSO
Anisomycin
SF
GSC827
C
SF-Input
SF-IP (Anti-ATP5α)
KDa
STS
CypD
ANT1/2
ATP5α
D
SF-Cytosol
SF-Mitochondria
AT3
AT20
KDa
CypD
1.0
0.1
0.6
ATP5α-AT20
ATP5α-AT3
TOM20

Figure S4

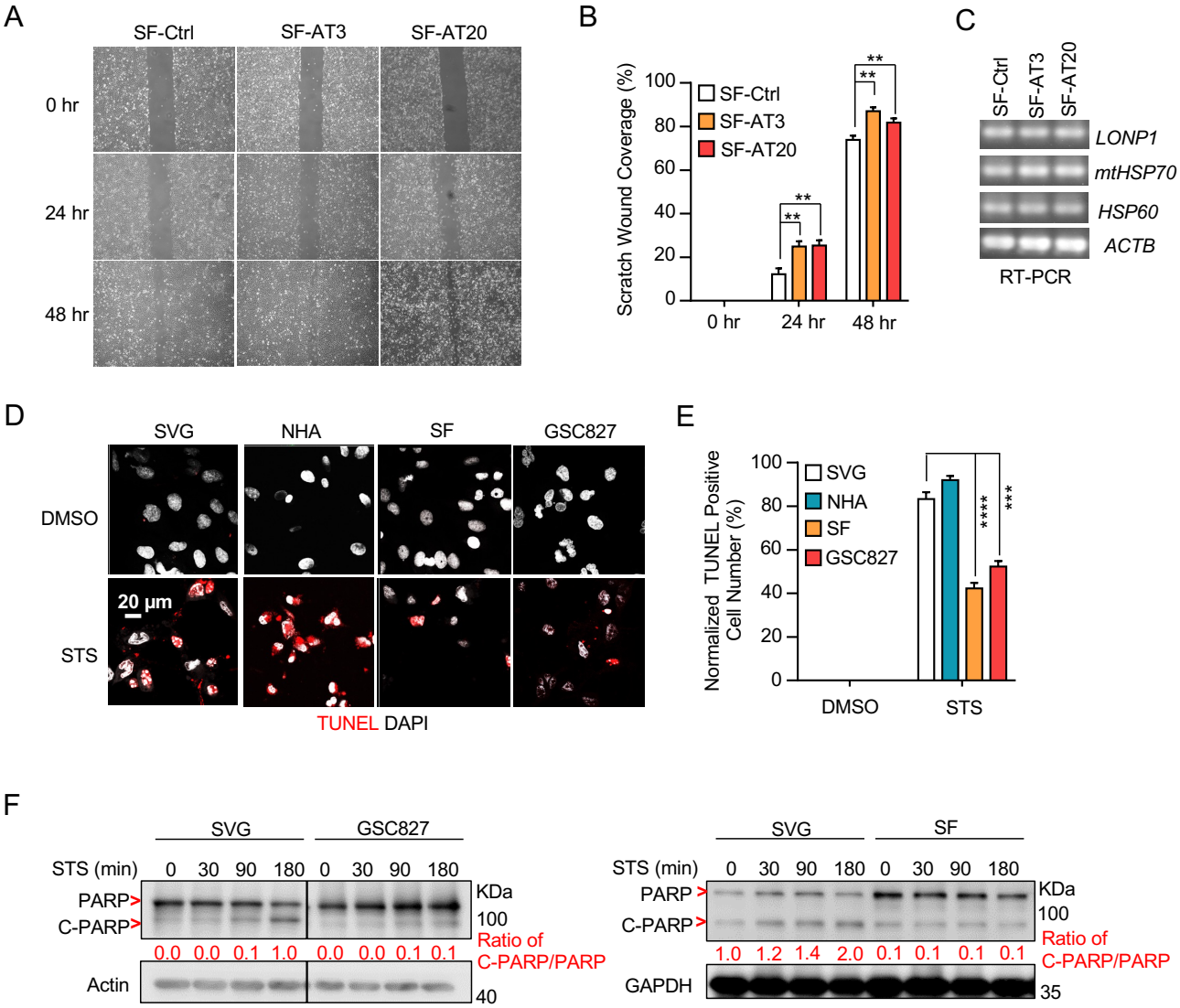
A
SF-Ctrl
SF-AT3
SF-AT20
0 hr
24 hr
48 hr
B
Scratch Wound Coverage (%)
100
80
60
40
20
0
SF-Ctrl
SF-AT3
SF-AT20
**
**
**
**
0 hr
24 hr
48 hr
C
SF-Ctrl
SF-AT3
SF-AT20
LONP1
mtHSP70
HSP60
ACTB
RT-PCR
D
SVG
NHA
SF
GSC827
DMSO
STS
20 μm
TUNEL DAPI
E
Normalized TUNEL Positive Cell Number (%)
100
80
60
40
20
0
SVG
NHA
SF
GSC827
****
***
DMSO
STS
F
SVG
GSC827
STS (min)
0 30 90 180 0 30 90 180
PARP
C-PARP
KDa
100
Ratio of C-PARP/PARP
0.0 0.0 0.1 1.0 0.0 0.0 0.1 0.1
Actin
40
SVG
SF
STS (min)
0 30 90 180 0 30 90 180
PARP
C-PARP
KDa
100
Ratio of C-PARP/PARP
1.0 1.2 1.4 2.0 0.1 0.1 0.1 0.1
GAPDH
35

Figure S5

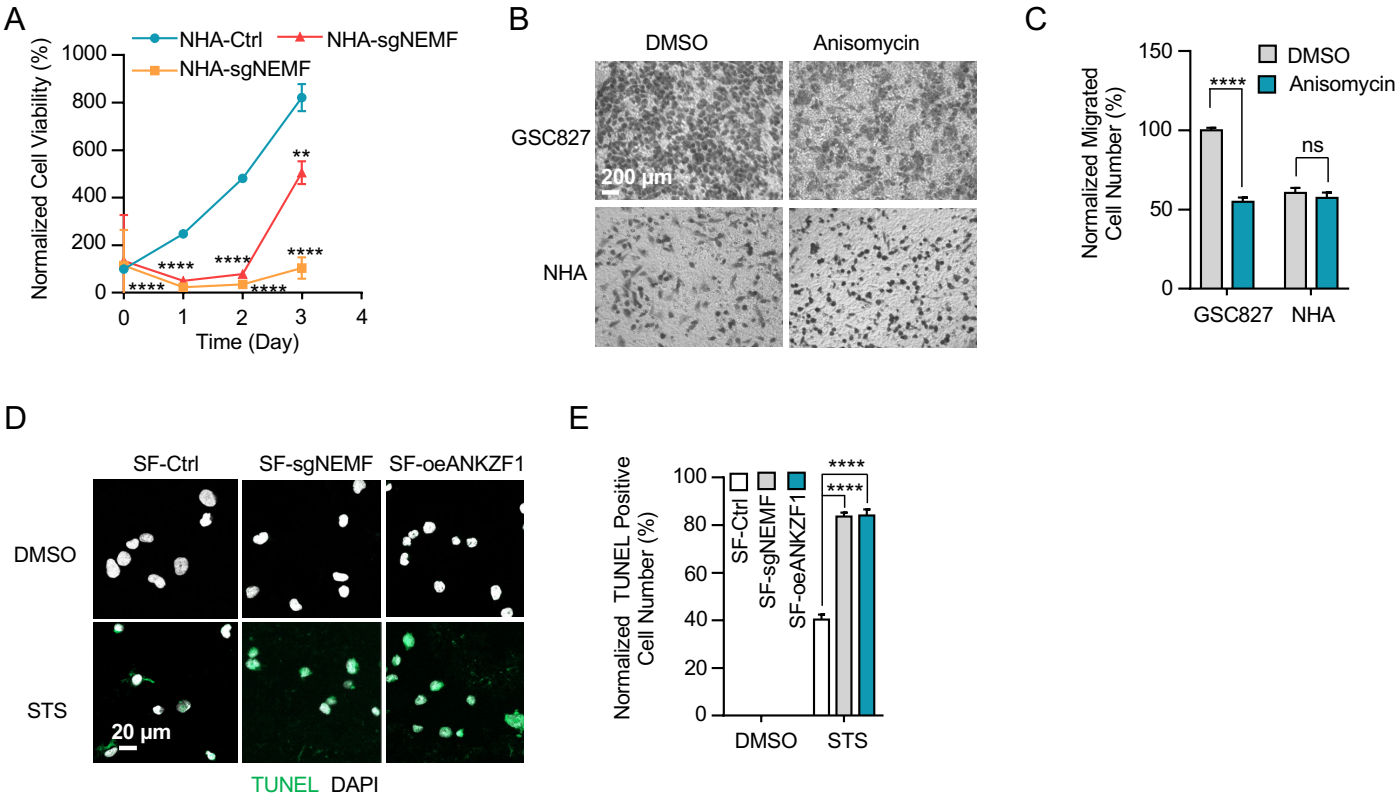
A
NHA-Ctrl
NHA-sgNEMF
NHA-sgNEMF
Normalized Cell Viability (%)
1000
800
600
400
200
0
0
1
2
3
4
Time (Day)
****
****
****
****
**
B
DMSO
Anisomycin
GSC827
NHA
200 μm
C
DMSO
Anisomycin
Normalized Migrated Cell Number (%)
150
100
50
0
****
ns
GSC827
NHA
D
SF-Ctrl
SF-sgNEMF
SF-oeANKZF1
DMSO
STS
20 μm
TUNEL DAPI
E
Normalized TUNEL Positive Cell Number (%)
100
80
60
40
20
0
SF-Ctrl
SF-sgNEMF
SF-oeANKZF1
****
****
DMSO
STS